

Robust Kronecker Component Analysis

Mehdi Bahri, *Student Member, IEEE*, Yannis Panagakis, and Stefanos Zafeiriou, *Member, IEEE*

Abstract—Dictionary learning and component analysis models are fundamental in learning compact representations that are relevant to a given task (feature extraction, dimensionality reduction, denoising, etc.). The model complexity is encoded by means of specific structure, such as sparsity, low-rankness, or nonnegativity. Unfortunately, approaches like K-SVD - that learn dictionaries for sparse coding via Singular Value Decomposition (SVD) - are hard to scale to high-volume and high-dimensional visual data, and fragile in the presence of outliers. Conversely, robust component analysis methods such as the Robust Principle Component Analysis (RPCA) are able to recover low-complexity (e.g., low-rank) representations from data corrupted with noise of unknown magnitude and support, but do not provide a dictionary that respects the structure of the data (e.g., images), and also involve expensive computations. In this paper, we propose a novel Kronecker-decomposable component analysis model, coined as Robust Kronecker Component Analysis (RKCA), that combines ideas from sparse dictionary learning and robust component analysis. RKCA has several appealing properties, including robustness to gross corruption; it can be used for low-rank modeling, and leverages separability to solve significantly smaller problems. We design an efficient learning algorithm by drawing links with a restricted form of tensor factorization, and analyze its optimality and low-rankness properties. The effectiveness of the proposed approach is demonstrated on real-world applications, namely background subtraction and image denoising and completion, by performing a thorough comparison with the current state of the art.

Index Terms—Component Analysis, Dictionary Learning, Separable Dictionaries, Low-rank, Sparsity, Global Optimality.

1 INTRODUCTION

COMPONENT analysis models and representation learning methods can be traced back to Principal Component Analysis [1], [2]. Since then a rich set of statistical models and algorithms tailored to learn compact representations from data have been developed. The building block of such methods is some sort of structured matrix or tensor factorization, allowing to learn components or representations that are relevant to a given task, e.g., feature extraction, dimensionality reduction, clustering, classification, denoising, etc. The model complexity is encoded by means of low-rankness or over-completeness, and physical level constraints are enforced by imposing a specific structure, such as sparsity or nonnegativity. The importance of learned components and representations cannot be overstated, and neither can their efficiency in dramatically improving machine perception. Prominent examples are Convolutional Neural Networks [3], [4], which through hierarchical feature extraction build ad-hoc representations enabling state of the art performance on a wide range of problems [5].

In this work, we study models and optimization algorithms for the unsupervised learning of compact representations from data. In particular, the proposed Robust Kronecker Component Analysis (RKCA) method, offers to bridge (multilinear) Robust PCA [6], [7] and Sparse Dictionary Learning [8], [9] from the perspective of a robust low-rank tensor factorization.

1.1 Robust PCA and sparse dictionary learning

Assuming a set of N data samples $\mathbf{x}_1, \dots, \mathbf{x}_n \in \mathbb{R}^m$ represented as the columns of a matrix \mathbf{X} , structured matrix factorization seeks to decompose \mathbf{X} into meaningful components of a given structure, by solving a regularization problem of the form:

$$\min_{\mathbf{Z}} l(\mathbf{X}, \mathbf{Z}) + \lambda g(\mathbf{Z}), \quad (1)$$

where \mathbf{Z} is an approximation of the data with respect to a loss $l(\cdot)$, $g(\cdot)$ is a possibly non-smooth regularizer that encourages the desired structure, and $\lambda \geq 0$ is a regularization parameter balancing the two terms. Popular instances of (1) include Principal Component Analysis (PCA) [1], [2] and its variants, e.g., Sparse PCA [10], Robust PCA (RPCA) [11], as well as sparse dictionary learning [8], [9], [12].

Concretely, when \mathbf{Z} is taken to be factorized in the form $\mathbf{D}\mathbf{R}$, i.e., $\mathbf{Z} = \mathbf{D}\mathbf{R}$ we obtain a range of different models depending on the choice of the regularization and of the properties of \mathbf{D} . For instance, assuming $\mathbf{Z} = \mathbf{D}\mathbf{R}$ is a low-rank approximation of \mathbf{X} and $\lambda = 0$, (1) yields PCA, while by imposing sparsity on \mathbf{D} , Sparse PCA [10] is obtained. To handle data corrupted by sparse noise of large magnitude, RPCA [11] assumes that the observation matrix, \mathbf{X} , is the sum of a low-rank matrix \mathbf{A} and of a sparse matrix \mathbf{E} that collects the gross errors, or outliers. This model is actually a special instance of (1) when $\mathbf{Z} = \mathbf{A} + \mathbf{E}$, $g(\mathbf{Z}) = \|\mathbf{A}\|_* + \lambda \|\mathbf{E}\|_1$, and $l(\cdot)$ is the Frobenius norm. Here, $\|\cdot\|_*$ denotes the low-rank promoting nuclear norm and $\|\cdot\|_1$ denotes the ℓ_1 norm that enforces sparsity. Matrix RPCA has been extended to tensors in multiple ways, relying on varying definitions of the tensor rank. We refer to [6], [7] for an overview of CP-based and Tucker-based tensor RPCA models, and to Section 7 for specifics on the models compared in this paper.

• The authors are with the Department of Computing, Imperial College London, London, UK, SW7 2RH.
E-mail: mehdi.bahri15@imperial.ac.uk
• Y. Panagakis is also with Middlesex University London, UK.
• S. Zafeiriou is also with the University of Oulu, Finland.

Manuscript received April 19, 2005; revised August 26, 2015.

Assuming \mathbf{D} is over-complete and requiring $\mathbf{R} = [\mathbf{r}_1, \dots, \mathbf{r}_n]$ to be sparse, (1) leads to sparse dictionary learning by solving the non-convex optimization problem:

$$\min_{\mathbf{R}, \mathbf{D}} \|\mathbf{X} - \mathbf{D}\mathbf{R}\|_F^2 + \lambda \sum_{i=1}^n \|\mathbf{r}_i\|_0, \quad (2)$$

where $\|\cdot\|_F$ is the Frobenius norm and $\|\cdot\|_0$ is the ℓ_0 pseudo-norm, counting the number of non-zero elements. In K-SVD and its variants, problem (2) is solved in an iterative manner that alternates between sparse coding of the data samples on the current dictionary, and a process of updating the dictionary atoms to better fit the data using the Singular Value Decomposition (SVD) [13], [14]. This procedure suffers from a high computational burden, preventing the applicability of the method to high-dimensional and large scale data.

To overcome the issue of scalability in dictionary learning, a separable structure on the dictionary can be enforced. For instance, the Separable Dictionary Learning (SeDiL) [15] considers a set of samples in matrix form, namely, $\mathcal{X} = (\mathbf{X}_i)_i$, admitting sparse representations in bases \mathbf{A}, \mathbf{B} , which their Kronecker product constructs the dictionary. The separable dictionary learning is casted as:

$$\min_{\mathbf{A}, \mathbf{B}, \mathbf{R}} \frac{1}{2} \sum_i \|\mathbf{X}_i - \mathbf{A}\mathbf{R}_i\mathbf{B}^T\|_F^2 + \lambda g(\mathbf{R}) + \kappa r(\mathbf{A}) + \kappa r(\mathbf{B}), \quad (3)$$

where the regularizers $g(\cdot)$ and $r(\cdot)$ promote sparsity in the representations, and low mutual-coherence of the dictionary $\mathbf{D} = \mathbf{B} \otimes \mathbf{A}$, respectively. Here, \mathbf{D} is constrained to have orthogonal columns, i.e., the pair \mathbf{A}, \mathbf{B} shall lie on the product manifold of two product of sphere manifolds. A different approach is taken in [16]: a separable 2D dictionary is learnt in a two-step strategy similar to that of K-SVD. Each matrix observation \mathbf{X}_i is represented as $\mathbf{A}\mathbf{R}_i\mathbf{B}^T$. In the first step, the sparse representations \mathbf{R}_i are found by 2D Orthogonal Matching Pursuit (OMP) [17]. In the second step, a CP [18], [19] decomposition is performed on a tensor of residuals via Regularized Alternating Least Squares to solve $\min_{\mathbf{A}, \mathbf{B}, \mathbf{R}} \|\mathbf{X} - \mathbf{R} \times_1 \mathbf{A} \times_2 \mathbf{B}\|_F^2$.

1.2 Outline and contributions

Here, we propose novel methods for separable dictionary learning based on robust tensor factorizations that learn simultaneously the dictionary and the sparse representations. We do not seek overcompleteness, but rather promote low-rankness in a pair of dictionaries and sparsity in the codes to learn a low-rank representation of the input tensor. In this regard, our methods combine ideas from both Sparse Dictionary Learning and Robust PCA, as well as tensor factorizations. Our solvers are based on the Alternating Direction of Multipliers Method (ADMM) [20].

A preliminary version of this work has been presented in [21]. This paper offers the following novelties:

- We generalize the results of [21] to the RKCA problem and propose new regularizers that yield stronger optimality properties.
- We show that RKCA with these well-chosen regularizers can be reformulated in the framework of

1. cf. notations for the product \times_n

[22], [23] allowing us to provide global optimality guarantees. It is worth mentioning that our proof applies to any Tucker factorization problem.

- We demonstrate that RKCA can perform tensor completion in the presence of gross corruption.
- We derive a Linearized ADMM (LADMM) algorithm for RKCA to improve scalability.
- Finally, we offer two different perspectives on the low-rank promoting properties of RKCA.

The rest of manuscript is organized as follows. Section 2 is dedicated to deriving the RKCA model, relating RKCA to separable dictionary learning, and deriving RKCA with missing values. In Section 3, we discuss the optimality guarantees by formulating RKCA as an equivalent CP factorization with duplicated factors. Section 4 is dedicated to the LADMM variant for improved scalability. Perspectives on the low-rank promoting properties can be found in Section 5, and a discussion on the computational cost and implementation details of the methods in Section 6. Finally, we present in Section 7 experimental evidence of the effectiveness of RKCA on synthetic and real-world data.

2 MODEL DERIVATION

Throughout the paper, matrices (vectors) are denoted by uppercase (lowercase) boldface letters e.g., $\mathbf{X}, (\mathbf{x})$. \mathbf{I} denotes the identity matrix of compatible dimensions. The i^{th} column of \mathbf{X} is denoted as \mathbf{x}_i . Tensors are considered as the multidimensional equivalent of matrices (second-order tensors), and vectors (first-order tensors), and denoted by bold calligraphic letters, e.g., \mathcal{X} . The *order* of a tensor is the number of indices needed to address its elements. Consequently, each element of an M^{th} -order tensor \mathcal{X} is addressed by M indices, i.e., $(\mathcal{X})_{i_1, i_2, \dots, i_M} \doteq x_{i_1, i_2, \dots, i_M}$.

The sets of real and integer numbers are denoted by \mathbb{R} and \mathbb{Z} , respectively. An M^{th} -order real-valued tensor \mathcal{X} is defined over the tensor space $\mathbb{R}^{I_1 \times I_2 \times \dots \times I_M}$, where $I_m \in \mathbb{Z}$ for $m = 1, 2, \dots, M$.

The mode- n product of a tensor $\mathcal{X} \in \mathbb{R}^{I_1 \times I_2 \times \dots \times I_M}$ with a matrix $\mathbf{U} \in \mathbb{R}^{J \times I_n}$, denoted by $\mathcal{X} \times_n \mathbf{U}$, is defined element-wise as

$$(\mathcal{X} \times_m \mathbf{x})_{i_1, \dots, i_{n-1}, i_{n+1}, \dots, i_M} = \sum_{i_n=1}^{I_n} x_{i_1, i_2, \dots, i_M} x_{i_n}. \quad (4)$$

The *Kronecker* product of matrices $\mathbf{A} \in \mathbb{R}^{I \times K}$, and $\mathbf{B} \in \mathbb{R}^{L \times M}$, is denoted by $\mathbf{A} \otimes \mathbf{B}$, and yields a matrix of dimensions $I \cdot L \times K \cdot M$. The mode- n unfolding, or mode- n matricization, of a tensor \mathcal{X} will be written $\mathbf{X}_{[n]}$.

Finally, we define the tensor *Tucker rank* as the vector of the ranks of its mode- n unfoldings (i.e., its mode- n ranks), and the tensor *multi-rank* [24], [25] as the vector of the ranks of its frontal slices. More details about tensors, such as the definitions of tensor slices and mode- n unfoldings, can be found in [26] for example.

2.1 RKCA and Tensor RPCA

Consider a set of N two dimensional observations (i.e., matrices) $\mathbf{X}_i \in \mathbb{R}^{m \times n}$, $i = 1, \dots, N$ stacked as the frontal slices of a tensor \mathcal{X} . We study *Tensor Robust PCA* problems:

$$\begin{aligned} \min_{\mathbf{A}, \mathbf{B}, \mathcal{R}, \mathcal{E}} \quad & f(\mathcal{L}) + g(\mathcal{E}) \\ \text{s.t.} \quad & \mathcal{X} = \mathcal{L} + \mathcal{E}, \end{aligned} \quad (5)$$

where \mathcal{L} and \mathcal{E} are respectively the low-rank and sparse components of \mathcal{X} . We will define $f(\cdot)$ and $g(\cdot)$ to be regularization functions, possibly non-smooth and non-convex, meant to promote structural properties of \mathcal{L} and \mathcal{E} - in our case, low-rankness of \mathcal{L} , and sparsity in \mathcal{E} .

The Robust Kronecker Component Analysis (RKCA) is obtained by assuming \mathcal{L} factorizes in a restricted form of Tucker factorization, and defining $f(\cdot)$ as a combination of penalties on the factors. More specifically, we assume:

$$\mathcal{L} = \mathcal{R} \times_1 \mathbf{A} \times_2 \mathbf{B} \quad (6)$$

Figure 1 illustrates the decomposition.

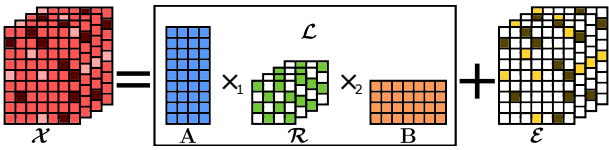


Fig. 1: Illustration of the decomposition.

We construct f to promote low-rankness in the first two modes of \mathcal{L} and therefore in each of its frontal slices. In this work, we will discuss three different choices of f depending on the *positive-homogeneity* degree of the full regularization.

Definition 2.1 (def. 3 of [23, page 6]). A function $\theta : \mathbb{R}^{D^1} \times \dots \times \mathbb{R}^{D^N} \rightarrow \mathbb{R}^D$ is **positively homogeneous with degree \mathbf{p}** if $\theta(\alpha x^1, \dots, \alpha x^N) = \alpha^p \theta(x^1, \dots, x^N)$, $\forall \alpha \geq 0$. Notably $\theta(0) = 0$ holds.

The following choice of f is the *degree 2 regularizer* and recovers the model presented in [21]:

$$f(\mathcal{L}) = \alpha \|\mathcal{R}\|_1 + \|\mathbf{B} \otimes \mathbf{A}\|_F \quad (7)$$

while choice:

$$f(\mathcal{L}) = \alpha \|\mathcal{R}\|_1 \|\mathbf{B} \otimes \mathbf{A}\|_* \quad (8)$$

and:

$$f(\mathcal{L}) = \alpha \|\mathcal{R}\|_1 \|\mathbf{B} \otimes \mathbf{A}\|_* \quad (9)$$

are *degree 3 regularizers*.

In all three cases, the regularizer comprises a norm on the Kronecker product of the Tucker factors, hence the proposed method is coined as RKCA. The interpretation of this will be made clear in Section 2.3.

2.2 An efficient algorithm for the degree 2 regularizer

In this section, we derive an efficient algorithm for the degree 2-regularized problem. This discussion will serve as a basis for the other regularizers which only require minor modifications of this algorithm.

Choosing f to be (7) and g to be the element-wise ℓ_1 norm we obtain the constrained optimization problem

$$\begin{aligned} \min_{\mathbf{A}, \mathbf{B}, \mathcal{R}, \mathcal{E}} \quad & \alpha \|\mathcal{R}\|_1 + \lambda \|\mathcal{E}\|_1 + \|\mathbf{B} \otimes \mathbf{A}\|_F \\ \text{s.t.} \quad & \mathcal{X} = \mathcal{R} \times_1 \mathbf{A} \times_2 \mathbf{B} + \mathcal{E}, \end{aligned} \quad (10)$$

where \mathcal{R} is a tensor whose i^{th} frontal slice encodes the representation of \mathbf{X}_i on a column basis \mathbf{A} and a row basis \mathbf{B} . We impose $r \in \mathbb{N}$, $r \leq \min(m, n)$ as a natural *upper bound* on the rank of each frontal slice of \mathcal{L} and on its mode-1 and mode-2 ranks:

$$\mathbf{L}_i = \mathbf{A} \mathcal{R}_i \mathbf{B}^\top \quad (11)$$

Hence, $\mathbf{A} \in \mathbb{R}^{m \times r}$, $\mathbf{B} \in \mathbb{R}^{n \times r}$, and $\mathcal{R} \in \mathbb{R}^{r \times r \times N}$.

Problem (10) is not jointly convex, but is convex in each component individually. We resort to an alternating-direction method and propose a non-convex ADMM procedure that operates on the frontal slices.

Minimizing $\|\mathbf{B} \otimes \mathbf{A}\|_F$ presents a challenge: the product is high-dimensional, the two bases are coupled, and the loss is non-smooth. Let $\|\cdot\|_p$ denotes the Schatten- p norm². Using the identity $\|\mathbf{A} \otimes \mathbf{B}\|_p = \|\mathbf{A}\|_p \|\mathbf{B}\|_p$ ³ and remarking that $\|\mathbf{B}\|_F \|\mathbf{A}\|_F \leq \frac{\|\mathbf{A}\|_F^2 + \|\mathbf{B}\|_F^2}{2}$, we minimize a simpler upper bound⁴. The resulting sub-problems are smaller, and therefore more easy to solve computationally. In order to obtain exact proximal steps for the encodings \mathbf{R}_i , we introduce a split variable \mathbf{K}_i such that $\forall i$, $\mathbf{K}_i = \mathbf{R}_i$. Thus, we solve:

$$\begin{aligned} \min_{\mathbf{A}, \mathbf{B}, \mathcal{R}, \mathcal{E}} \quad & \alpha \|\mathcal{R}\|_1 + \lambda \|\mathcal{E}\|_1 + \frac{1}{2} (\|\mathbf{A}\|_F^2 + \|\mathbf{B}\|_F^2) \\ \text{s.t.} \quad & \mathcal{X} = \mathcal{K} \times_1 \mathbf{A} \times_2 \mathbf{B} + \mathcal{E} \\ \text{s.t.} \quad & \mathcal{R} = \mathcal{K} \end{aligned} \quad (12)$$

By introducing the Lagrange multipliers Λ and \mathbf{Y} , such that the i^{th} frontal slice corresponds to the i^{th} constraint, and the dual step sizes μ and $\mu_\mathcal{K}$, we formulate the Augmented Lagrangian of problem (12):

$$\begin{aligned} L(\mathbf{A}, \mathbf{B}, \mathcal{R}, \mathcal{E}, \Lambda, \mathbf{Y}, \mu, \mu_\mathcal{K}) = & \lambda \sum_i \|\mathbf{R}_i\|_1 + \lambda \sum_i \|\mathbf{E}_i\|_1 + \\ & \frac{1}{2} (\|\mathbf{A}\|_F^2 + \|\mathbf{B}\|_F^2) + \sum_i \langle \Lambda_i, \mathbf{X}_i - \mathbf{A} \mathbf{K}_i \mathbf{B}^\top - \mathbf{E}_i \rangle + \\ & \sum_i \langle \mathbf{Y}_i, \mathbf{R}_i - \mathbf{K}_i \rangle + \frac{\mu}{2} \sum_i \|\mathbf{X}_i - \mathbf{A} \mathbf{K}_i \mathbf{B}^\top - \mathbf{E}_i\|_F^2 + \\ & \frac{\mu_\mathcal{K}}{2} \sum_i \|\mathbf{R}_i - \mathbf{K}_i\|_F^2 \end{aligned} \quad (13)$$

We can now derive the ADMM updates. Each \mathbf{E}_i is given by shrinkage after rescaling [11]:

$$\mathbf{E}_i = \mathcal{S}_{\lambda/\mu}(\mathbf{X}_i - \mathbf{A} \mathbf{K}_i \mathbf{B}^\top + \frac{1}{\mu} \Lambda_i) \quad (14)$$

A similar rule is immediate to derive for \mathbf{R}_i , and solving for \mathbf{A} and \mathbf{B} is straightforward with some matrix algebra. We therefore focus on the computation of the split variable \mathbf{K}_i . Differentiating, we find \mathbf{K}_i satisfies:

$$\begin{aligned} \mu_\mathcal{K} \mathbf{K}_i + \mu \mathbf{A}^\top \mathbf{A} \mathbf{K}_i \mathbf{B}^\top \mathbf{B} \\ = \mathbf{A}^\top (\Lambda_i + \mu(\mathbf{X}_i - \mathbf{E}_i)) \mathbf{B} + \mu_\mathcal{K} \mathbf{R}_i + \mathbf{Y}_i \end{aligned} \quad (15)$$

The key is here to recognize equation (15) is a *Stein equation*, and can be solved in cubical time and quadratic space in r by solvers for discrete-time Sylvester equations - such as the Hessenberg-Schur method [28] - instead of the naive $O(r^6)$ time, $O(r^4)$ space solution of vectorizing the equation in a size r^2 linear system. We obtain Algorithm 1.

2. The Schatten- p norm of \mathbf{A} is the ℓ_p norm of its singular values.
3. From the compatibility of the Kronecker product with the SVD.
4. $\|\mathbf{AB}^\top\|_*$ [27].

Algorithm 1 RKCA with degree 2 regularization.

```

1: procedure RKCA( $\mathcal{X}, r, \lambda, \alpha$ )
2:    $\mathbf{A}^0, \mathbf{B}^0, \mathcal{E}^0, \mathcal{R}^0, \mathcal{K}^0, \Lambda^0, \mathbf{Y}^0, \mu^0, \mu_{\mathcal{K}}^0 \leftarrow \text{INITIALIZE}(\mathcal{X})$ 
3:   while not converged do
4:      $\mathcal{E}^{t+1} \leftarrow \mathcal{S}_{\lambda/\mu^t}(\mathcal{X} - \mathcal{K}^t \times_1 \mathbf{A}^t \times_2 \mathbf{B}^t + \frac{1}{\mu^t} \Lambda^t)$ 
5:      $\tilde{\mathcal{X}}^{t+1} \leftarrow \mathcal{X} - \mathcal{E}^{t+1}$ 
6:      $\mathbf{A}^{t+1} \leftarrow (\sum_i (\mu^t \tilde{\mathbf{X}}_i^{t+1} + \Lambda_i^t) \mathbf{B}^t (\mathbf{K}_i^t)^\top) / (\mathbf{I} + \mu^t \sum_i \mathbf{K}_i^t (\mathbf{B}^t)^\top \mathbf{B}^t (\mathbf{K}_i^t)^\top)$ 
7:      $\mathbf{B}^{t+1} \leftarrow (\sum_i (\mu^t \tilde{\mathbf{X}}_i^{t+1} + \Lambda_i^t)^\top \mathbf{A}^{t+1} \mathbf{K}_i^t) / (\mathbf{I} + \mu^t \sum_i (\mathbf{K}_i^t)^\top (\mathbf{A}^{t+1})^\top \mathbf{A}^{t+1} \mathbf{K}_i^t)$ 
8:     for all  $i$  do
9:        $\mathbf{K}_i^{t+1} \leftarrow \text{STEIN}(-\frac{\mu^t}{\mu_{\mathcal{K}}^t} (\mathbf{A}^{t+1})^\top \mathbf{A}^{t+1}, (\mathbf{B}^{t+1})^\top \mathbf{B}^{t+1},$ 
           $\frac{1}{\mu_{\mathcal{K}}^t} [(\mathbf{A}^{t+1})^\top (\Lambda_i^t + \mu^t \tilde{\mathbf{X}}_i^{t+1}) \mathbf{B}^{t+1} + \mathbf{Y}_i^t] + \mathbf{R}_i^t)$ 
10:       $\mathbf{R}_i^{t+1} \leftarrow \mathcal{S}_{\alpha/\mu_{\mathcal{K}}^t}(\mathbf{K}_i^{t+1} - \frac{1}{\mu_{\mathcal{K}}^t} \mathbf{Y}_i^t)$ 
11:    end for
12:     $\Lambda^{t+1} \leftarrow \Lambda^t + \mu^t (\tilde{\mathcal{X}}^{t+1} - \mathcal{K}^{t+1} \times_1 \mathbf{A}^{t+1} \times_2 \mathbf{B}^{t+1})$ 
13:     $\mathcal{Y}^{t+1} \leftarrow \mathcal{Y}^t + \mu_{\mathcal{K}}^t (\mathcal{R}^{t+1} - \mathcal{K}^{t+1})$ 
14:     $\mu^{t+1} \leftarrow \min(\mu^*, \rho \mu^t)$ 
15:     $\mu_{\mathcal{K}}^{t+1} \leftarrow \min(\mu_{\mathcal{K}}^*, \rho \mu_{\mathcal{K}}^t)$ 
16:  end while
17:  return  $\mathbf{A}, \mathbf{B}, \mathcal{R}, \mathcal{E}$ 
18: end procedure

```

2.3 Robust Separable Dictionary Learning

In this section, we show RKCA learns structured robust dictionaries by tensor factorization. We do not seek overcompleteness, but rather promote sparsity in the dictionary to learn a low-rank representation of the input tensor. In this regard, our methods combine ideas from both Sparse Dictionary Learning and Tensor Robust PCA, and the choice of the Kronecker product is explained.

Consider the following Sparse Dictionary Learning problem with Frobenius-norm regularization on the dictionary \mathbf{D} , where we decompose N observations $\mathbf{x}_i \in \mathbb{R}^{mn}$ on $\mathbf{D} \in \mathbb{R}^{mn \times r_1 r_2}$ with representations $\mathbf{r}_i \in \mathbb{R}^{r_1 r_2}$:

$$\min_{\mathbf{D}, \mathbf{R}} \sum_i \|\mathbf{x}_i - \mathbf{D}\mathbf{r}_i\|_2^2 + \lambda \sum_i \|\mathbf{r}_i\|_1 + \|\mathbf{D}\|_{\text{F}} \quad (16)$$

We assume a Kronecker-decomposable dictionary $\mathbf{D} = \mathbf{B} \otimes \mathbf{A}$ with $\mathbf{A} \in \mathbb{R}^{m \times r_1}, \mathbf{B} \in \mathbb{R}^{n \times r_2}$. To model the presence of outliers, we introduce a set of vectors $\mathbf{e}_i \in \mathbb{R}^{mn}$ and, with $d = r_1 r_2 + mn$, define the block vectors and matrices:

$$\mathbf{y}_i = \begin{bmatrix} \mathbf{r}_i \\ \mathbf{e}_i \end{bmatrix} \in \mathbb{R}^d \quad \mathbf{C} = [\mathbf{B} \otimes \mathbf{A} \quad \mathbf{I}] \in \mathbb{R}^{mn \times d} \quad (17)$$

We obtain a two-level structured dictionary \mathbf{C} and the associated sparse encodings \mathbf{y}_i . Breaking-down the variables to reduce dimensionality and discarding $\|\mathbf{I}\|_{\text{F}}$:

$$\begin{aligned} & \min_{\mathbf{A}, \mathbf{B}, \mathbf{R}, \mathbf{E}} \sum_i \|\mathbf{x}_i - (\mathbf{B} \otimes \mathbf{A})\mathbf{r}_i - \mathbf{e}_i\|_2^2 \\ & + \lambda \sum_i \|\mathbf{r}_i\|_1 + \lambda \sum_i \|\mathbf{e}_i\|_1 + \|\mathbf{B} \otimes \mathbf{A}\|_{\text{F}} \end{aligned} \quad (18)$$

Suppose now that the observations \mathbf{x}_i were obtained by vectorizing two-dimensional data such as images, i.e., $\mathbf{x}_i = \text{vec}(\mathbf{X}_i), \mathbf{X}_i \in \mathbb{R}^{m \times n}$. We find preferable to keep the observations in matrix form as this preserves the spatial structure of the images (and, as explained in Section 2.2, allows us solve matrix equations efficiently instead of high-dimensional linear systems). Without loss of generality, we

choose $r_1 = r_2 = r$ and $\mathbf{r}_i = \text{vec}(\mathbf{R}_i), \mathbf{R}_i \in \mathbb{R}^{r \times r}$, and recast the problem as:

$$\begin{aligned} & \min_{\mathbf{A}, \mathbf{B}, \mathbf{R}, \mathcal{E}} \sum_i \|\mathbf{X}_i - \mathbf{A}\mathbf{R}_i \mathbf{B}^\top - \mathbf{E}_i\|_{\text{F}}^2 \\ & + \lambda \sum_i \|\mathbf{R}_i\|_1 + \lambda \sum_i \|\mathbf{E}_i\|_1 + \|\mathbf{B} \otimes \mathbf{A}\|_{\text{F}} \end{aligned} \quad (19)$$

Equivalently, enforcing the equality constraints and concatenating the matrices $\mathbf{X}_i, \mathbf{R}_i$, and \mathbf{E}_i as the frontal slices of 3-way tensors, we obtain problem (10).

2.4 Tensor completion with RKCA

We now present an extension to the original problem where we assume we are only given incomplete and possibly grossly-corrupted observations. Given a set $\Omega \subset \mathbb{N}^{I_1 \times I_2 \times \dots \times I_N}$ we define the sampling operator $\pi_{\Omega} : \mathbb{R}^{I_1 \times I_2 \times \dots \times I_N} \rightarrow \mathbb{R}^{I_1 \times I_2 \times \dots \times I_N}$ as the projection on the space of N -way tensors whose only non-zero entries are indexed by N -tuples in Ω , i.e., $\forall \mathcal{X} \in \mathbb{R}^{I_1 \times I_2 \times \dots \times I_N}$:

$$\pi_{\Omega}(x_{i_1, i_2, \dots, i_N}) = \begin{cases} 1 & (i_1, i_2, \dots, i_N) \in \Omega \\ 0 & (i_1, i_2, \dots, i_N) \notin \Omega \end{cases}$$

It is simple to show π_{Ω} is an orthogonal projection. Clearly, π_{Ω} is linear and idempotent ($\pi_{\Omega} \circ \pi_{\Omega} = \pi_{\Omega}$). A tensor \mathcal{X} is in the null space of π_{Ω} if and only if none of its non-zero entries are indexed by N -tuples of Ω . Denote by $\bar{\Omega}$ the complement of Ω , we have $\forall \mathcal{X}, \langle \pi_{\Omega}(\mathcal{X}), \pi_{\bar{\Omega}}(\mathcal{X}) \rangle = 0$.

With partial observations, we solve:

$$\begin{aligned} & \min_{\mathbf{A}, \mathbf{B}, \mathbf{R}} \quad f(\mathcal{L}) + \|\mathcal{E}\|_1 \\ & \text{s.t.} \quad \pi_{\Omega}(\mathcal{X}) = \pi_{\Omega}(\mathcal{L}) + \pi_{\Omega}(\mathcal{E}) \end{aligned} \quad (20)$$

By the orthogonality of π_{Ω} , $\|\mathcal{E}\|_1 = \|\pi_{\Omega}(\mathcal{E})\|_1 + \|\pi_{\bar{\Omega}}(\mathcal{E})\|_1$. Without loss of generality we follow [7], [29] and assume $\pi_{\bar{\Omega}}(\mathcal{X}) = 0$ such that $\pi_{\bar{\Omega}}(\mathcal{X}) = \pi_{\bar{\Omega}}(\mathcal{L}) + \pi_{\bar{\Omega}}(\mathcal{E})$. This implies that we do not seek to recover possible corruption on the missing values but directly the missing element. Problem (20) is therefore equivalent to:

$$\begin{aligned} & \min_{\mathbf{A}, \mathbf{B}, \mathbf{R}} \quad f(\mathcal{L}) + \|\pi_{\Omega}(\mathcal{E})\|_1 \\ & \text{s.t.} \quad \mathcal{X} = \mathcal{L} + \mathcal{E} \end{aligned} \quad (21)$$

To solve (21) we need to compute the proximal operator of $\|\pi_{\Omega}(\mathcal{E})\|_1$, we show (proof in Appendix A.1) that the corresponding operator is the selective shrinkage $\mathcal{S}_{\lambda}^{\Omega}$:

$$\forall \mathcal{X} \in \mathbb{R}^{I_1 \times I_2 \times \dots \times I_N}, \mathcal{S}_{\lambda}^{\Omega}(\mathcal{X}) = \mathcal{S}_{\lambda}(\pi_{\Omega}(\mathcal{X})) + \pi_{\bar{\Omega}}(\mathcal{X}) \quad (22)$$

From the previous developments, we argue that extending our algorithms to handle missing value only involves using the selective shrinkage operator in the update of \mathcal{E} .

We present tensor completion results in Section 7.4.

3 RKCA AND GLOBAL OPTIMALITY

The work of [22], [23] suggests global optimality can be achieved from any initialization in tensor factorization models given that the factorization and regularization mappings match in certain ways. We summarize the main results of this work and show our model with regularizer (8) or (9) respects the conditions for global optimality.

3.1 Review of the main results

We first review some of the concepts manipulated in [22], [23] and give an overview of the main results.

Definition 3.1 (def. 1 of [23, page 6]). A **size- r set of K factors** $(\mathcal{X}^1, \dots, \mathcal{X}^K)_r$ is defined to be a set of K tensors where the final dimension of each tensor is equal to r . This is to be interpreted $(\mathcal{X}^1, \dots, \mathcal{X}^K)_r \in \mathbb{R}^{(D^1 \times r)} \times \dots \times \mathbb{R}^{(D^K \times r)}$.

Definition 3.2 (def. 6 of [23, page 6]). An **elemental mapping**, $\phi : \mathbb{R}^{D^1} \times \dots \times \mathbb{R}^{D^K} \rightarrow \mathbb{R}^D$ is any mapping which is positively homogeneous with degree $p \neq 0$. The **r -element factorization mapping** $\Phi_r : \mathbb{R}^{(D^1 \times r)} \times \dots \times \mathbb{R}^{(D^K \times r)} \rightarrow \mathbb{R}^D$ is defined as:

$$\Phi_r(\mathcal{X}^1, \dots, \mathcal{X}^K) = \sum_{i=1}^r \phi(\mathcal{X}_i^1, \dots, \mathcal{X}_i^K). \quad (23)$$

Definition 3.3 (def. 7 of [23, page 8]). An **elemental regularization function** $g : \mathbb{R}^{D^1} \times \dots \times \mathbb{R}^{D^K} \rightarrow \mathbb{R}_+ \cup \infty$, is defined to be any function which is positive semidefinite and positively homogeneous.

Definition 3.4 (def. 8 of [23, page 9]). Given an elemental mapping ϕ and an elemental regularization function g , the authors define (ϕ, g) to be a **nondegenerate pair** if 1) g and ϕ are both positively homogeneous with degree p , for some $p \neq 0$ and 2) $\forall X \in \text{Im}(\phi) \setminus \{0\}, \exists \mu \in (0, \infty]$ and $(\tilde{z}^1, \dots, \tilde{z}^K)$ such that $\phi(\tilde{z}^1, \dots, \tilde{z}^K) = X, g(\tilde{z}^1, \dots, \tilde{z}^K) = \mu$, and $g(z^1, \dots, z^K) \geq \mu$ for all (z^1, \dots, z^K) such that $\phi(z^1, \dots, z^K) = X$.

The main result of their paper provides a characterization of the global optima of CP-based tensor factorization problems. We quote Theorem 15 of [23].

Theorem 3.5 (theorem 15 of [23, page 15]). *Given a function $f_r(\mathcal{X}^1, \dots, \mathcal{X}^K, Q)$, any local minimizer of the optimization problem:*

$$\min_{(\mathcal{X}^1, \dots, \mathcal{X}^K)_r, Q} f_r(\mathcal{X}^1, \dots, \mathcal{X}^K, Q) \equiv \quad (24)$$

$$\ell(\Phi_r(\mathcal{X}^1, \dots, \mathcal{X}^K), Q) + \lambda \sum_{i=1}^r g(\mathcal{X}_i^1, \dots, \mathcal{X}_i^K) + H(Q)$$

such that $(\mathcal{X}_{i_0}^1, \dots, \mathcal{X}_{i_0}^K) = (0, \dots, 0)$ for some $i_0 \in \{1, \dots, r\}$ is a global minimizer.

Where Q is an optional set of non-factorized variables (in our case \mathcal{E}), H is convex possibly non-smooth, $\ell(\cdot)$ is jointly convex and once-differentiable in (\mathcal{X}, Q) , and (ϕ, g) is a nondegenerate pair.

In order to apply the results of [22], [23] to our case, we describe a reduction of our factorization that allows it to fit in the framework. The arguments we develop below can easily be extended to the general case of the Tucker factorization.

3.2 Definitions on integer sequences

Let us first define in a clear manner the concepts of periodic and group-periodic integer sequences.

Definition 3.6. An integer sequence a_1, a_2, \dots, a_n is said to be periodic with period p (i.e. p -periodic) if:

$$\forall i \geq 1, a_i = a_{i+p} \quad (25)$$

We will need to manipulate sequences of periodic patterns of repeating number, for this purpose we define a group periodic sequence as follows.

Definition 3.7. We will say an integer sequence a_1, a_2, \dots, a_n is group periodic with group length l and period p , or (l, p) -group periodic, if:

$$\forall i \geq 1, a_i = a_{i+pl} \quad (26)$$

And:

$$\forall k \geq 0, \forall l k + 1 \leq i, j \leq l(k + 1), a_i = a_j \quad (27)$$

For instance, 110022110022 is $(2, 3)$ -group periodic.

3.3 The factorization function

The main challenge in adapting our model to the framework of [22], [23] is to find a factorization function that can be expressed as a sum of elemental mappings. Problem (10) as is does not lend itself to such a formulation: even though the factors \mathbf{A} and \mathbf{B} form a size- r set of 2 factors, the core tensor \mathcal{R} is of size N on its last dimension. We note however that the set of frontal slices of \mathcal{R} is a size- r set of N factors, but this formulation doesn't satisfy Proposition 10 of [23] and it is not immediately obvious how to define concatenation of the factors of \mathcal{X} and \mathcal{Y} and how to verify the convexity of the factorization-regularization function Ω (equation (18) and Proposition 11 of [23] omitted here for brevity). Additionally, the results of [22], [23] have been proved in the case of a single sum over the last dimension of the factors, but our factorization being a special case of Tucker decomposition is most naturally described as:

$$\mathcal{L} = \mathcal{R} \times_1 \mathbf{A} \times_2 \mathbf{B} \quad (28)$$

$$= \mathcal{R} \times_1 \mathbf{A} \times_2 \mathbf{B} \times_3 \mathbf{I}_N \quad (29)$$

$$= \sum_i \sum_j \sum_k r_{i,j,k} \cdot \mathbf{a}_i \otimes \mathbf{b}_j \otimes \mathbf{c}_k \quad (30)$$

First, we observe that the order of the sums can be permuted such that it is clear that our model expresses \mathcal{L} as the sum of N tensors of size $m \times n \times N$ where all frontal slices are the null matrix except for one:

$$\mathcal{L} = \sum_k \sum_i \sum_j r_{i,j,k} \cdot \mathbf{a}_i \otimes \mathbf{b}_j \otimes \mathbf{c}_k \quad (31)$$

$$\text{Since } (\mathbf{c}_k)_i = \delta_{i,k} = \begin{cases} 1 & i = j \\ 0 & i \neq j \end{cases}.$$

Next, we seek a transformation such that (31) does not involve cross-terms. Our idea is to unfold the Tucker factorization by duplicating elements of the factors to express it in the form (23) where the sum is over a size- s set of 3 factors (or M factors for the general Tucker).

Since the sum involves all Nr^2 elements of \mathcal{R} it is clear such an unfolding must too. Since there are respectively r , r , and N columns in \mathbf{A} , \mathbf{B} , and \mathbf{I}_N and $\max(r, N, Nr^2) = Nr^2$, we have $s = Nr^2$.

We define a bijection from \mathbb{N}^3 to \mathbb{N} such that each triple index (i, j, k) is mapped to a unique positive integer l by setting, in the general M -dimensional Tucker case:

$$l = 1 + \sum_{k=1}^M (i_k - 1) J_k \quad \text{and} \quad L_k = \prod_{m=1}^{k-1} D_m, \quad (32)$$

where D_m denotes the dimension along mode m . In our case we have $D_1 = r$, $D_2 = r$, $D_3 = N$. This re-indexing corresponds to the standard definition of the vec operator where the columns of each frontal slice of the 3-way tensor are stacked in order.

We now describe the new factors of our decomposition:

- We define $\sigma = \text{vec}(\mathcal{R})$
- We construct $\tilde{\mathbf{A}}$ and $\tilde{\mathbf{B}}$ from \mathbf{A} and \mathbf{B} by duplicating columns
- \mathbf{I}_N doesn't depend on the data and can be injected directly in the elemental mapping

The construction of $\tilde{\mathbf{A}}$ and $\tilde{\mathbf{B}}$ must be consistent with the ordering of the elements in the re-indexing. For the reader's convenience, we visualize in table (1) the correspondence in the simple case where $r = 2$ and $N = 3$. To map back l to i ,

l	1	2	3	4	5	6	7	8	9	10	11	12
i	1	2	1	2	1	2	1	2	1	2	1	2
j	1		2		1		2		1		2	
k		1			2				3			

TABLE 1: Illustration of our re-indexing in a small-dimensional case.

j, k we observe the 3 sequences are (group) periodic. In fact, the sequence corresponding to the innermost sum of (28) is (r^2, N) -group periodic. We find that:

$$k = (\lceil \frac{l}{r^2} \rceil - 1) \bmod N + 1 \quad (33)$$

The sequence for j is (r, r) -group periodic and the sequence for i is r -periodic, so we have:

$$j = (\lceil \frac{l}{r} \rceil - 1) \bmod r + 1 \quad (34)$$

And:

$$i = (l - 1) \bmod r + 1 \quad (35)$$

The augmented factors all have dimension Nr^2 over their last mode. For $\tilde{\mathbf{A}}$ we duplicate each column $Nr^2 - r$ times by concatenating Nr copies of \mathbf{A} on the column dimension. For $\tilde{\mathbf{B}}$, each column is copied $r - 1$ times before stacking the next column, and the resulting matrix is concatenated N times. The $\tilde{\mathbf{c}}_l$ are defined by:

$$(\tilde{\mathbf{c}}_l)_i = \delta_{i, (\lceil \frac{l}{r^2} \rceil - 1) \bmod N + 1} \quad (36)$$

The elemental mapping of our factorization is therefore:

$$\phi(\sigma, \tilde{\mathbf{a}}, \tilde{\mathbf{b}}) = \sigma \cdot \tilde{\mathbf{a}} \otimes \tilde{\mathbf{b}} \otimes \delta_{., (\lceil \frac{l}{r^2} \rceil - 1) \bmod N + 1} \quad (37)$$

And the factorization function is defined over the size Nr^2 set of 3 factors $(\sigma, \tilde{\mathbf{A}}, \tilde{\mathbf{B}})$ by:

$$\Phi_{Nr^2}(\sigma, \tilde{\mathbf{A}}, \tilde{\mathbf{B}}) = \sum_{l=1}^{Nr^2} \sigma_l \cdot \tilde{\mathbf{a}}_l \otimes \tilde{\mathbf{b}}_l \otimes \delta_{l, (\lceil \frac{l}{r^2} \rceil - 1) \bmod r^2 + 1} \quad (38)$$

3.4 RKCA with degree 3 regularization

Having established that our factorization function can be reformulated to fit within the framework of [22], [23] we check that the *degree 3 regularizers* introduced in Section 2 are compatible. Recall both regularizers are of the form:

$$g(\mathcal{L}) = \alpha \|\mathcal{R}\|_1 \|\mathbf{A}\|_q \|\mathbf{B}\|_q \quad (39)$$

With $\|\cdot\|_p$ the Schatten- p norm, $p = 1$ for the Nuclear norm and $p = 2$ for the Frobenius norm. As we shall see in Section 5.2, g is low-rank promoting.

In the case of the Frobenius penalty, the resulting optimization problem is:

$$\begin{aligned} \min_{\mathbf{A}, \mathbf{B}, \mathcal{R}, \mathcal{E}} \quad & \lambda \|\mathcal{R}\|_1 \|\mathbf{B}\|_{\text{F}} \|\mathbf{A}\|_{\text{F}} + \lambda \|\mathcal{E}\|_1 \\ \text{s.t.} \quad & \mathcal{X} = \mathcal{R} \times_1 \mathbf{A} \times_2 \mathbf{B} + \mathcal{E} \end{aligned} \quad (40)$$

The regularizer g adapted to our transformation is:

$$g(\sigma, \tilde{\mathbf{A}}, \tilde{\mathbf{B}}) = \|\sigma\|_1 \frac{\|\tilde{\mathbf{A}}\|_{\text{F}} \|\tilde{\mathbf{B}}\|_{\text{F}}}{Nr} \quad (41)$$

This stems from the fact that the Frobenius norm is equivalent to the element-wise ℓ_2 norm, and each element of \mathbf{A} and \mathbf{B} appears Nr times in $\tilde{\mathbf{A}}$ and $\tilde{\mathbf{B}}$.

In the case of the Nuclear norm, we simply observe that the numbers of linearly independent columns in $\tilde{\mathbf{A}}$ and $\tilde{\mathbf{B}}$ are clearly the same as in \mathbf{A} and \mathbf{B} , so our transformation preserves the ranks of the target matrices, and the regularization function is simply:

$$g(\sigma, \tilde{\mathbf{A}}, \tilde{\mathbf{B}}) = \|\sigma\|_1 \|\tilde{\mathbf{A}}\|_* \|\tilde{\mathbf{B}}\|_* \quad (42)$$

It should be clear that the newly defined ϕ and g are both positively homogeneous of degree 3, and form a nondegenerate pair. Property 10 of [23] also holds. Hence, we argue that RKCA with a product of norms regularization enjoys the optimality guarantees presented in [23].

4 LINEARIZED ADMM FOR SCALABILITY

The substitution method used in Section 2.2 is effective in practice but comes with an additional cost that limits its scalability. Notably, the cost of solving a Stein equation for each frontal slice of \mathcal{R} cannot be neglected in practice. Additionally, the added parameters can make tuning difficult. Linearization provides an alternative approach that can scale better to large dimensions and large datasets, in this section, we show how it can be applied to our models.

We state the linearized updates for \mathbf{A} , \mathbf{B} , and \mathcal{R} . The development for \mathcal{R} can directly be applied to solving problem (10) and its variants with a simple change in the shrinkage factor. Detailed derivations can be found in Appendix C.

4.1 Updating the core \mathcal{R}

From the augmented Lagrangian of problem (40), updating \mathcal{R} requires solving the minimization problem:

$$\begin{aligned} \min_{\mathcal{R}} \quad & \alpha \|\mathbf{A}\|_{\text{F}} \|\mathbf{B}\|_{\text{F}} \|\mathcal{R}\|_1 + \\ & \frac{\mu}{2} \|\mathcal{X} - \mathcal{R} \times_1 \mathbf{A} \times_2 \mathbf{B} - \mathcal{E} + \frac{1}{\mu} \mathbf{A}\|_{\text{F}}^2 \end{aligned} \quad (43)$$

Let $\Delta = \mathcal{X} - \mathcal{E} + \frac{1}{\mu} \Lambda$, we show the updated \mathcal{R}^{t+1} is:

$$\mathcal{S}_{\alpha'} \left(\mathcal{R}^t - \frac{1}{L_{\mathcal{R}}} [(\mathcal{R}^t \times_1 \mathbf{A} \times_2 \mathbf{B}) - \Delta] \times_1 \mathbf{A}^T \times_2 \mathbf{B}^T \right) \quad (44)$$

Where $L_{\mathcal{R}} \geq \sigma_{\max}^2(\mathbf{B}) \cdot \sigma_{\max}^2(\mathbf{A})$ and $\alpha' = \alpha$ for problem (10) and $\alpha' = \alpha \|\mathbf{A}\|_{\text{F}} \|\mathbf{B}\|_{\text{F}}$ for problem (40).

4.2 Updating A and B

The sub-problem for \mathbf{A} is:

$$\begin{aligned} \min_{\mathbf{A}} \alpha \|\mathbf{A}\|_{\text{F}} \|\mathbf{B}\|_{\text{F}} \|\mathcal{R}\|_1 + \\ \frac{\mu}{2} \|\mathcal{X} - \mathcal{R} \times_1 \mathbf{A} \times_2 \mathbf{B} - \mathcal{E} + \frac{1}{\mu} \Lambda\|_{\text{F}}^2 \end{aligned} \quad (45)$$

Our problem is separable in the frontal slices of \mathcal{X} and therefore in the frontal slices of the components of the factorization and of the Lagrange multipliers. Using the same Δ notation from the update of \mathcal{R} and denoting $\mathbf{C}_i = \mathbf{R}_i \mathbf{B}^T$:

$$\mathbf{A}^* = \operatorname{argmin}_{\mathbf{A}} \left[\frac{\alpha}{\mu} \right] \|\mathbf{A}\|_{\text{F}} + \frac{1}{2} \sum_i \|\Delta_i - \mathbf{A} \mathbf{C}_i\|_{\text{F}}^2 \quad (46)$$

Let $a = \frac{1}{\mu L_{\mathbf{A}}} (\alpha \|\mathbf{B}^T\|_{\text{F}} \|\mathcal{R}^t\|_1)$, we have:

$$\mathbf{A}^{t+1} = \operatorname{prox}_{a \|\cdot\|_{\text{F}}} \left(\mathbf{A}^t - \frac{1}{L_{\mathbf{A}}} \sum_i (\mathbf{A}^t \mathbf{C}_i^t - \Delta_i^t) \mathbf{C}_i^T \right) \quad (47)$$

$$L_{\mathbf{A}} \geq \|\sum_i \mathbf{C}_i \mathbf{C}_i^T\|_{\text{F}} = \sum_i \|\mathbf{C}_i \mathbf{C}_i^T\|_{\text{F}} = \sum_i \|\mathbf{R}_i \mathbf{B}^T \mathbf{B} \mathbf{R}_i^T\|_{\text{F}}.$$

Similarly, letting $\mathbf{D}_i^t = \mathbf{A}^{t+1} \mathbf{R}_i \quad \forall i$ and $b = \frac{1}{\mu L_{\mathbf{B}}} (\alpha \|\mathbf{A}^{t+1}\|_{\text{F}} \|\mathcal{R}^t\|_1)$ we find:

$$\mathbf{B}^{t+1} = \operatorname{prox}_{b \|\cdot\|_{\text{F}}} \left(\mathbf{B}^t - \frac{1}{L_{\mathbf{B}}} \sum_i (\mathbf{D}_i^t \mathbf{B}^{t+1} - \Delta_i^t)^T \mathbf{D}_i^t \right) \quad (48)$$

$$L_{\mathbf{B}} \geq \|\sum_i \mathbf{D}_i^T \mathbf{D}_i\|_{\text{F}} = \sum_i \|\mathbf{R}_i^T \mathbf{A}^T \mathbf{A} \mathbf{R}_i\|_{\text{F}}.$$

Remark that $\mathcal{C} = \mathcal{R} \times_2 \mathbf{B}$ then $L_{\mathbf{A}} = \|\mathbf{C}_{[2]} \mathbf{C}_{[2]}^T\|_{\text{F}}$ where $\mathbf{C}_{[2]}$ is the mode-2 matricization of \mathcal{C} . The i^{th} line of $\mathbf{C}_{[2]}$ is the concatenation of the i^{th} columns of all the frontal slices of \mathcal{C} so $\mathbf{C}_{[2]} \mathbf{C}_{[2]}^T$, the matrix of the dot products of the lines of $\mathbf{C}_{[2]}$, captures interactions across the i^{th} rows of all the input images. Conversely, $\mathcal{D} = \operatorname{permute}(\mathcal{R} \times_1 \mathbf{A}, [2, 1, 3])$, so $L_{\mathbf{B}} = \|\mathbf{D}_{[2]} \mathbf{D}_{[2]}^T\|_{\text{F}}$ where $\mathbf{D}_{[2]}$ is the mode-2 matricization of \mathcal{D} . The i^{th} line of $\mathbf{D}_{[2]}$ is the concatenation of the i^{th} lines of all the frontal slices of \mathcal{D} so $\mathbf{D}_{[2]} \mathbf{D}_{[2]}^T$, the matrix of the dot products of the lines of $\mathbf{D}_{[2]}$, captures interactions across the i^{th} columns of all the input images.

5 RKCA LEARNS LOW-RANK DICTIONARIES

In this Section we explain the low-rank promoting behavior of RKCA from two complementary perspective. First, we show that the regularizers defined in equations (7), (8), and (9) directly provide upper bounds on the mode-1 and mode-2 ranks of the low-rank component, and thus on the sub-rank of each of its frontal slices. This perspective was first presented in [21]. The second approach to explaining the models' properties studies the optimization sub-problems associated with the two bases \mathbf{A} and \mathbf{B} . Based on recent work [30], we show these sub-problems are equivalent to rank-minimization problems and admit closed-form solutions that involve forms of singular value thresholding.

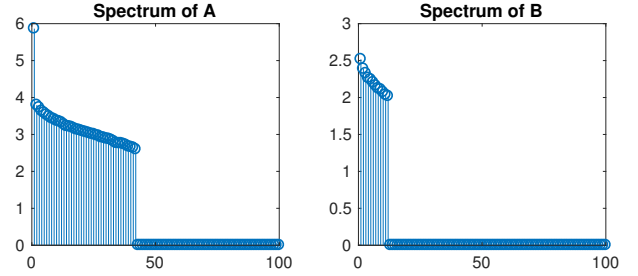


Fig. 2: Sample spectra of \mathbf{A} and \mathbf{B} . Ground truth attained ($\mathbf{A}: 42$, $\mathbf{B}: 12$). $r = 100$. Degree 2 regularizer.

5.1 Low-rank solutions

Seeing the models from the perspective of Robust PCA, which seeks a low-rank representation \mathbf{A} of the dataset \mathbf{X} , we minimize the rank of the low-rank tensor \mathcal{L} . More precisely, we show in theorem 5.1 that we simultaneously penalize the Tucker rank and the multi-rank of \mathcal{L} .

Theorem 5.1. RKCA encourages low mode-1 and mode-2 rank, and thus, low-rankness in each frontal slice of \mathcal{L} , for suitable choices of the parameters λ and α .

Proof. We minimize either $\lambda \|\mathcal{E}\|_1 + \alpha \|\mathcal{R}\|_1 + \|\mathbf{A} \otimes \mathbf{B}\|_{\text{F}}$, $\lambda \|\mathcal{E}\|_1 + \alpha \|\mathcal{R}\|_1 \|\mathbf{A} \otimes \mathbf{B}\|_{\text{F}}$, or $\lambda \|\mathcal{E}\|_1 + \alpha \|\mathcal{R}\|_1 \|\mathbf{A} \otimes \mathbf{B}\|_{*}$. From the equivalence of norms in finite-dimensions, $\exists k \in \mathbb{R}_+, \|\mathbf{A} \otimes \mathbf{B}\|_* \leq k \|\mathbf{A} \otimes \mathbf{B}\|_{\text{F}}$. In the case of the Frobenius norm, we can choose $\alpha = \frac{\alpha'}{k}, \lambda = \frac{\lambda'}{k}$ to reduce the problem to that of the nuclear norm. In all cases, we penalize $\operatorname{rank}(\mathbf{A} \otimes \mathbf{B}) = \operatorname{rank}(\mathbf{A}) \operatorname{rank}(\mathbf{B})$. Given that the rank is a non-negative integer, $\operatorname{rank}(\mathbf{A})$ or $\operatorname{rank}(\mathbf{B})$ decreases necessarily. Therefore, we minimize the mode-1 and mode-2 ranks of $\mathcal{L} = \mathcal{R} \times_1 \mathbf{A} \times_2 \mathbf{B}$. Additionally, $\forall i, \operatorname{rank}(\mathbf{A} \mathbf{R}_i \mathbf{B}^T) \leq \min(\operatorname{rank}(\mathbf{A}), \operatorname{rank}(\mathbf{B}), \operatorname{rank}(\mathbf{R}_i))$.

Exhibiting a valid k may help in the choice of parameters. We show $\forall \mathbf{A} \in \mathbb{R}^{m \times n}, \|\mathbf{A}\|_* \leq \sqrt{\min(m, n)} \|\mathbf{A}\|_{\text{F}}$: We know $\forall \mathbf{x} \in \mathbb{R}^n, \|\mathbf{x}\|_1 \leq \sqrt{n} \|\mathbf{x}\|_2$. Recalling the nuclear norm and the Frobenius norm are the Schatten-1 and Schatten-2 norms, and \mathbf{A} has $\min(m, n)$ singular values, the result follows. \square

In practice, we find that on synthetic data designed to test the models, we effectively recover the ranks of \mathbf{A} and \mathbf{B} regardless of the choice of r , as seen in Figure 2.

5.2 Another perspective on rank minimization

We present an alternative interpretation of the low-rank properties of our methods. In [30] the authors show that Frobenius norm and Nuclear norm regularizations either lead to the same optimal solution - even in the presence of noise - when the dictionary provides enough representative power, or are equivalent in the sense that they describe two different bases on the column space of the dictionary. We explain the behavior of our algorithms by showing the sub-problems in \mathbf{A} and \mathbf{B} are rank-minimization problems.

5.2.1 Sub-problems in A and B

For generality purposes, let us begin with the problem:

$$\begin{aligned} \min_{\mathbf{A}, \mathbf{B}, \mathcal{R}, \mathcal{E}} \quad & \beta \|\mathbf{A}\|_{\text{F}} \|\mathbf{B}\|_{\text{F}} + \lambda \|\mathcal{E}\|_1 + Q \\ \text{s.t.} \quad & \mathcal{X} = \mathcal{R} \times_1 \mathbf{A} \times_2 \mathbf{B} \times_3 \mathbf{I}_N + \mathcal{E} \end{aligned} \quad (49)$$

For the degree 3 regularizer we have $\beta = \alpha \|\mathcal{R}\|_1$ and $Q = 0$, for the degree 2 case we have $\beta = 1$ and $Q = \alpha \|\mathcal{R}\|_1$. We omit the dependency in \mathcal{R} for β and Q as they are constants when solving the sub-problems in \mathbf{A} and \mathbf{B} .

The sub-problem in \mathbf{A} is:

$$\begin{aligned} \min_{\mathbf{A}} \quad & [\beta \|\mathbf{B}\|_{\text{F}}] \|\mathbf{A}\|_{\text{F}} \\ \text{s.t.} \quad & \mathcal{X} = \mathcal{R} \times_1 \mathbf{A} \times_2 \mathbf{B} \times_3 \mathbf{I}_N + \mathcal{E} \end{aligned} \quad (50)$$

We remind the reader of the following property of tensors and their matricizations:

$$(\mathcal{X} \times_{i=1}^N \mathbf{U}_i)_{[n]} = \mathbf{U}_n \mathbf{X}_{[n]} (\otimes_{i=N, i \neq n}^1 \mathbf{U}_i)^{\top} \quad (51)$$

Equivalently, in an matricized way:

$$\begin{aligned} \min_{\mathbf{A}} \quad & [\beta \|\mathbf{B}\|_{\text{F}}] \|\mathbf{A}\|_{\text{F}} \\ \text{s.t.} \quad & \mathbf{X}_{[1]} = \mathbf{A} \mathbf{R}_{[1]} (\mathbf{I}_N \otimes \mathbf{B})^{\top} + \mathbf{E}_{[1]} \end{aligned} \quad (52)$$

Noting that $\|\mathbf{A}\|_{\text{F}} = \|\mathbf{A}^{\top}\|_{\text{F}}$ we reformulate the problem in the form of equation (4) of [30]:

$$\begin{aligned} \min_{\mathbf{A}} \quad & \gamma \|\mathbf{A}^{\top}\|_{\text{F}} \\ \text{s.t.} \quad & \tilde{\mathbf{X}}_{[1]}^{\top} = \mathbf{D}_{\mathbf{A}} \mathbf{A}^{\top} \end{aligned} \quad (53)$$

With $\tilde{\mathbf{X}}_{[1]}^{\top} = \mathbf{X}_{[1]}^{\top} - \mathbf{E}_{[1]}^{\top}$, $\gamma = [\beta \|\mathbf{B}\|_{\text{F}}]$, $\mathbf{D}_{\mathbf{A}} = (\mathbf{I}_N \otimes \mathbf{B}) \mathbf{R}_{[1]}^{\top}$. The sub-problem in \mathbf{B} is very similar:

$$\begin{aligned} \min_{\mathbf{B}} \quad & [\beta \|\mathbf{A}\|_{\text{F}}] \|\mathbf{B}\|_{\text{F}} \\ \text{s.t.} \quad & \mathcal{X} = \mathcal{R} \times_1 \mathbf{A} \times_2 \mathbf{B} \times_3 \mathbf{I}_N + \mathcal{E} \end{aligned} \quad (54)$$

Matricizing on the second mode:

$$\begin{aligned} \min_{\mathbf{B}} \quad & \kappa \|\mathbf{B}^{\top}\|_{\text{F}} \\ \text{s.t.} \quad & \tilde{\mathbf{X}}_{[2]}^{\top} = \mathbf{D}_{\mathbf{B}} \mathbf{B}^{\top} \end{aligned} \quad (55)$$

With $\tilde{\mathbf{X}}_{[2]}^{\top} = \mathbf{X}_{[2]}^{\top} - \mathbf{E}_{[2]}^{\top}$, $\kappa = [\beta \|\mathbf{A}\|_{\text{F}}]$, $\mathbf{D}_{\mathbf{B}} = (\mathbf{I}_N \otimes \mathbf{A}) \mathbf{R}_{[2]}^{\top}$.

5.2.2 Optimal solutions and interpretation

According to [31] the optimal solution of $\min \|\mathbf{C}\|_{*}$ s.t. $\mathbf{X} = \mathbf{DC}$ assuming feasible solutions exist and $\mathbf{D} \neq \mathbf{0}$ is $\mathbf{C}^* = \mathbf{V}_r \mathbf{\Sigma}_r \mathbf{V}_r^{\top}$ where $\mathbf{U}_r \mathbf{\Sigma}_r \mathbf{V}_r^{\top}$ is the skinny SVD of \mathbf{D} . [32] showed it is also the optimal solution of $\min \|\mathbf{C}\|_{\text{F}}$ s.t. $\mathbf{X} = \mathbf{DC}$.

It is therefore easy to show that the optimal solution of $\min \|\mathbf{C}^{\top}\|_{*}$ s.t. $\mathbf{X} = \mathbf{DC}^{\top}$ under similar conditions is $\mathbf{U}_r \mathbf{U}_r^{\top}$.

Proof. Letting $\mathbf{X} = \mathbf{U} \mathbf{\Sigma} \mathbf{V}^{\top}$ we have $\mathbf{X}^{\top} = \mathbf{V} \mathbf{\Sigma} \mathbf{U}^{\top}$. \square

Letting $\mathbf{U}_p^{\mathbf{A}} \mathbf{\Sigma}_p^{\mathbf{A}} \mathbf{V}_p^{\mathbf{A}\top}$ the skinny SVD of $\mathbf{D}_{\mathbf{A}}$ and $\mathbf{U}_q^{\mathbf{B}} \mathbf{\Sigma}_q^{\mathbf{B}} \mathbf{V}_q^{\mathbf{B}\top}$ the skinny SVD of $\mathbf{D}_{\mathbf{B}}$ the optimal solutions for \mathbf{A} and \mathbf{B} are therefore $\mathbf{U}_p^{\mathbf{A}} \mathbf{U}_p^{\mathbf{A}\top}$ and $\mathbf{U}_q^{\mathbf{B}} \mathbf{U}_q^{\mathbf{B}\top}$.

For the sake of brevity, we shall describe the interpretation for \mathbf{A} as the same holds for \mathbf{B} by symmetry. It should be noted that $\mathbf{U}_p^{\mathbf{A}}$ is the PCA basis of $\mathbf{D}_{\mathbf{A}}$ and that $\mathbf{U}_p^{\mathbf{A}} \mathbf{U}_p^{\mathbf{A}\top}$ is the matrix of the orthogonal projection onto that basis. Thus, the optimal \mathbf{A} is the projection of $\mathbf{D}_{\mathbf{A}}$ onto its principal components. Remembering that $\mathbf{D}_{\mathbf{A}} = (\mathbf{I}_N \otimes \mathbf{B}) \mathbf{R}_{[1]}^{\top}$, $\mathbf{D}_{\mathbf{A}}$ is the product of \mathbf{B} with each code \mathbf{R}_i matricized such that the i^{th} line of $\mathbf{D}_{\mathbf{A}}$ is the concatenation of all the i^{th} columns of all the partial reconstructions $\mathbf{R}_k \mathbf{B}^{\top}$, and all the columns of $\mathbf{D}_{\mathbf{A}}$ are all the lines of the $\mathbf{R}_k \mathbf{B}^{\top}$, which can be seen as

the partial reconstruction of the low-rank images in their common row space $\text{Span}(\mathbf{B})$.

Hence, we can see the process of updating \mathbf{A} and \mathbf{B} as alternating PCAs in the row and column spaces, respectively.

6 IMPLEMENTATION DETAILS AND COMPLEXITY

In this Section, we discuss the computational complexity of our algorithms, the tuning of their parameters, and explain choices we made based on this discussion.

6.1 Computational complexity

The time and space complexity per iteration of Algorithm 1 (i.e. with the degree two regularizer) are $O(N(mnr + (m+n)r + mn + \min(m, n)r^2 + r^3 + r^2))$ and $O(N(mn + r^2) + (m+n)r + r^2)$. Since $r \leq \min(m, n)$, the terms in r are asymptotically negligible, but in practice it is useful to know how the computational requirements scale with the size of the dictionary. Similarly, the initialization procedure has cost $O(N(mn \min(m, n) + (\min(m, n))^3 + mn) + mn)$ in time and needs quadratic space per slice, assuming a standard algorithm is used for the SVD [33].

Switching to an LADMM update for \mathcal{R} eliminates the need of solving costly Stein equations. The soft-shrinkage operator is applied to the tensor $(\mathcal{R} \times_1 \mathbf{A} \times_2 \mathbf{B} - \Delta) \times_1 \mathbf{A}^{\top} \times_2 \mathbf{B}^{\top}$, which has Nr^2 elements, and can be computed in $O(N(\min(m, n)r^2 + mn + r^2 + r^3) + mr^2 + nr^2)$ by remembering that $(\mathcal{X} \times_1 \mathbf{A}) \times_1 \mathbf{B} = \mathcal{X} \times_1 \mathbf{BA}$. The space complexity of the update is $O(N(\min(m, n)r + r^2) + r^2)$.

Updating \mathbf{A} and \mathbf{B} with a Frobenius or with a nuclear norm penalty requires computing a proximal operator and also solving a linear system for ADMM with substitution. We focus on the computation of the proximal operator in Section 6.2. The substitution adds an additional time and space complexity of $O(mr + nr)$.

Several key steps in the algorithms, such as summations of independent terms, are trivially distributed in a *MapReduce* [34] way. Proximal operators are separable in nature and are therefore parallelizable. Consequently, highly parallel and distributed implementations are possible, and computational complexity can be further reduced by adaptively adopting sparse linear algebra structures and algorithms.

6.2 Frobenius and nuclear norm penalties

In equation (12) we used an upper bound on $\|\mathbf{A}\|_{\text{F}} \|\mathbf{B}\|_{\text{F}}$ to obtain smooth sub-problems. In the degree 3-regularized case, we must keep $g(\cdot)$ positive homogeneous of degree 3 and therefore cannot apply the same bound. Given the non-smoothness of the Frobenius norm, we must resort to other approaches such as substitution or linearization (c.f. Section 4 and Appendix B). We may thus choose to penalize the ranks of \mathbf{A} and \mathbf{B} directly with $\|\mathbf{A}\|_{*}$ and $\|\mathbf{B}\|_{*}$.

In Section 5.2, we then showed how Frobenius and Nuclear norm penalties can yield the same optimal solutions, and how in our case they would be equivalent in solving the sub-problems associated with \mathbf{A} and \mathbf{B} . It is therefore natural to wonder why we should choose one over the other, and what the practical implications of this choice are.

It can be shown that the proximal operator of the Schatten- p norm has a closed form expression that requires the computation of the SVD of the matrix (Proposition A.1, Appendix A.2). Computing the SVD is costly, with a typical algorithm [33] requiring $O(mn \min(m, n) + (\min(m, n))^3)$ floating-point operations. Storing the resulting triple $(\mathbf{U}, \mathbf{S}, \mathbf{V})$ requires $m \times \min(m, n) + \min(m, n)^2 + n \times \min(m, n)$ space. Although faster algorithms have been developed, scalability remains a concern.

However, the Frobenius norm is also the element-wise ℓ_2 norm of the matrix, whose proximal operator is only the projection on the unit ball and doesn't require any costly matrix decomposition. The choice of the Frobenius norm is therefore justified in the high dimensional setting.

6.3 Parameter tuning and adaptive ADMM

A key concern with the practical implementation of ADMM and LADMM algorithms is parameter tuning and initialization, and is exacerbated by the introduction of additional variables and constraints. A constraint of the form $\mathbf{X} = \mathbf{Y}$ translates to additional terms $\langle \Lambda, \mathbf{X} - \mathbf{Y}, + \rangle \frac{\mu}{2} \|\mathbf{X} - \mathbf{Y}\|_F^2$ in the augmented Lagrangian of the problem, where Λ is a tensor of Lagrange multipliers of the dimension of \mathbf{X} , and μ is a penalty parameter. In standard (L)ADMM, μ is initialized and updated such that the sequence $(\mu^t)_{t \geq 1}$ is bounded and non-decreasing, generally through a simple update $\mu^{t+1} = \rho\mu^t$. The initial value μ^0 and the value of ρ directly influence the speed of convergence and the quality of the reconstructed images. As more constraints are added, more penalty parameters are introduced and must be tuned and updated properly, possibly independently from one another. Although the literature on ADMM with adaptive penalty updates [35], [36], [37] suggests adaptive updates for the ρ variables, these solutions also come with their added complexity and possibly with more parameters to tune. In the case of LADMM, the practitioner must also ensure an adequate choice of value is made to upper bound the Lipschitz constants of the gradients in each update.

Due to the sensitivity of the ADMM and LADMM algorithms to parameter tuning, we found that the algorithm that provided the most benefits in practice and the best reconstructions was the one that was the simplest to tune. This explains our choice of Algorithm 1 and its LADMM variant for the experiments.

6.4 Convergence and initialization

Problems (10) and (40) are non-convex, therefore global convergence is a priori not guaranteed. Recent work [38], [39] studies the convergence of ADMM for non-convex and possibly non-smooth objective functions with linear constraints. Here, the constraints are not linear. We proposed problem (10) based on [22], [23] so global convergence could theoretically be attained with a local descent algorithm. However, problem (10) doesn't offer any guarantees and in both cases the (L)ADMM scheme employed does not necessarily converge to a local minimum. In this section, we provide experimental results for Algorithm 1 and discuss the initialization strategy implemented for all the variants.

We propose a simple initialization scheme for Algorithm 1 and its variants adapted from [40]. We initialize

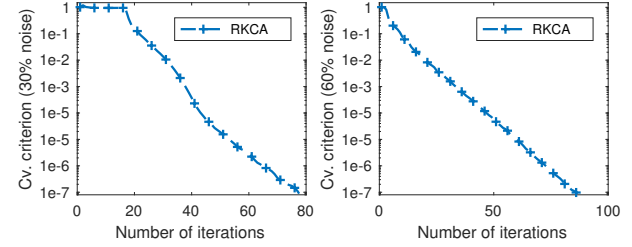


Fig. 3: Convergence on synthetic data with 30% and 60% corruption.

the bases \mathbf{A} and \mathbf{B} and the core \mathcal{R} by performing SVD on each observation $\mathbf{X}_i = \mathbf{U}_i \mathbf{S}_i \mathbf{V}_i^T$. We set $\mathbf{R}_i = \mathbf{S}_i$, $\mathbf{A} = \frac{1}{N} \sum_i \mathbf{U}_i$ and $\mathbf{B} = \frac{1}{N} \sum_i \mathbf{V}_i$. To initialize the dual-variables for the constraint $\mathbf{X}_i - \mathbf{A}\mathbf{R}_i\mathbf{B}^T - \mathbf{E}_i = \mathbf{0}$, we take $\mu^0 = \frac{\eta N}{\sum_i \|\mathbf{X}_i\|_F}$ where η is a scaling coefficient, chosen in practice to be $\eta = 1.25$ as in [40]. We chose $\mu_K^0 = \frac{\eta N}{\sum_i \|\mathbf{R}_i\|_F}$ and similarly for \mathbf{A} and \mathbf{B} when applicable. These correspond to averaging the initial values for each individual slice and its corresponding constraint. Our convergence criterion corresponds to primal-feasibility of problem (12) or (40), and is given by $\max(\text{err}_{\text{rec}}, \text{err}_{\mathcal{R}}, \text{err}_{\mathbf{A}}, \text{err}_{\mathbf{B}}) \leq \epsilon$ where $\text{err}_{\text{rec}} = \max_i \frac{\|\mathbf{X}_i - \mathbf{A}\mathbf{R}_i\mathbf{B}^T - \mathbf{E}_i\|_F^2}{\|\mathbf{X}_i\|_F^2}$ and $\text{err}_{\mathcal{R}} = \max_i \frac{\|\mathbf{R}_i - \mathbf{K}_i\|_F^2}{\|\mathbf{R}_i\|_F^2}$, $\text{err}_{\mathbf{A}} = \frac{\|\mathbf{A} - \mathbf{U}\|_F^2}{\|\mathbf{A}\|_F^2}$, and $\text{err}_{\mathbf{B}} = \frac{\|\mathbf{B} - \mathbf{V}\|_F^2}{\|\mathbf{B}\|_F^2}$. For the LADMM versions we only have $\max(\text{err}_{\text{rec}})$. Empirically, we obtained systematic convergence of Algorithm 1 to a good solution, and a linear convergence rate, as shown in Figure 3. Similar results were found for the ADMM with substitution algorithm for problem (40) and for the LADMM variants of both problems.

7 EXPERIMENTAL EVALUATION

We first provide experimental verification of the correctness of Algorithm 1 (with degree 2 regularization) on synthetic data. We then compared the performance of RKCA with degree 2 regularization against a range of state-of-the-art tensor decomposition algorithms on four low-rank modeling computer vision benchmarks: two for image denoising, and two for background subtraction. As a baseline, we report the performance of matrix Robust PCA implemented via inexact ALM (RPCA) [11], [40], and of Non-Negative Robust Dictionary Learning (RNNDL) [41]. We chose the following methods to include recent representatives of various existing approaches to low-rank modeling on tensors: The singleton version of Higher-Order Robust PCA (HORPCA-S) [7] optimizes the Tucker rank of the tensor through the sum of the nuclear norms of its unfoldings. In [42], the authors consider a similar model but with robust M-estimators as loss functions, either a Cauchy loss or a Welsh loss, and support both hard and soft thresholding; we tested the soft-thresholding models (Cauchy ST and Welsh ST). Non-convex Tensor Robust PCA (NC TRPCA) [43] adapts to tensors the matrix non-convex RPCA [44]. Finally, the two Tensor RPCA algorithms [24], [25] (TRPCA '14 and TRPCA '16) work with slightly different definitions of the tensor nuclear norm as a convex surrogate of the tensor multi-rank.

For each model, we identified a maximum of two parameters to tune via grid-search in order to keep parameter

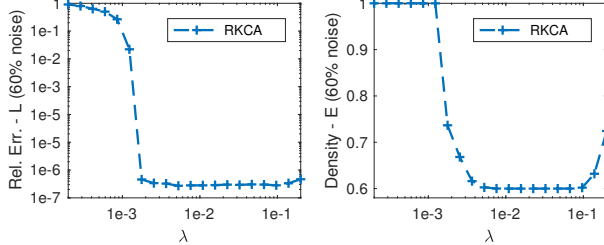


Fig. 4: Recovery performance with 60% corruption. Relative ℓ_2 error and density.

tuning tractable. When criteria or heuristics for choosing the parameters were provided by the authors, we chose the search space around the value obtained from them. In all cases, the tuning process explored a wide range of parameters to maximize performance.

When the performance of one method was significantly worse than that of the other, the result is not reported so as not to clutter the text (see Appendix E). This is the case of Separable Dictionary Learning [15] whose drastically different nature renders unsuitable for robust low-rank modeling, but was compared for completeness. For the same reason, we did not compare our method against K-SVD [13], or [16].

Finally, we provide tensor completion experiments with and without gross corruption in Section 7.4.

7.1 Validation on synthetic data

We generated synthetic data following the RKCA's assumptions by first sampling two random bases \mathbf{A} and \mathbf{B} of known ranks $r_{\mathbf{A}}$ and $r_{\mathbf{B}}$, N Gaussian slices for the core \mathcal{R} , and forming the ground truth $\mathcal{L} = \mathcal{R} \times_1 \mathbf{A} \times_2 \mathbf{B}$. We modeled additive random sparse Laplacian noise with a tensor \mathcal{E} whose entries are 0 with probability p , and 1 or -1 with equal probability otherwise. We generated data for $p = 70\%$ and $p = 40\%$, leading to a noise density of, respectively, 30% and 60%. We measured the reconstruction error on \mathcal{L} , \mathcal{E} , and the density of \mathcal{E} for varying values of λ , and $\alpha = 1 \times 10^{-2}$. Our model achieved near-exact recovery of both \mathcal{L} and \mathcal{E} , and exact recovery of the density of \mathcal{E} , for suitable values of λ . Evidence is presented in Figure 4 for the 60% noise case.

Algorithm 1 appears robust to small changes in λ , which suggests not only one value can lead to optimal results, and that a simple criterion that provides consistently good reconstruction may be derived, as in Robust PCA [11]. In the 30% noise case, we did not observe an increase in the density of \mathcal{E} as λ increases, and the ℓ_2 error on both \mathcal{E} and \mathcal{L} was of the order of 1×10^{-7} .

7.2 Background subtraction

Background subtraction is a common task in computer vision and can be tackled by robust low-rank modeling: the static or mostly static background of a video sequence can effectively be represented as a low-rank tensor while the foreground forms a sparse component of outliers.

7.2.1 Experimental procedure

We compared the algorithms on two benchmarks. The first is an excerpt of the *Highway* dataset [45], and consists in a

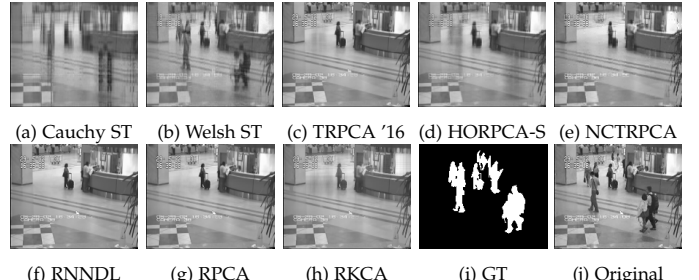


Fig. 5: Results on *Airport Hall*. TRPCA '14 removed.

video sequence of cars travelling on a highway; the background is completely static. We kept 400 gray-scale images re-sized to 48×64 pixels. The second is the *Airport Hall* dataset ([46]) and has been chosen as a more challenging benchmark since the background is not fully static and the scene is richer. We used the same excerpt of 300 frames (frames 3301 to 3600) as in [47], and kept the frames in their original size of 144×176 pixels.

We treat background subtraction as a binary classification problem. Since ground truth frames are available for our excerpts, we report the AUC [48] on both videos. The value of α was set to 1×10^{-2} for both experiments.

7.2.2 Results

We provide the original, ground truth, and recovered frames in Figure 5 for the *Hall* experiment (*Highway* in Appendix E).

Table 2 presents the AUC scores of the algorithms, ranked in order of their mean performance on the two benchmarks. The two matrix methods rank high on both benchmarks and only half of the tensor algorithms match or outperform this baseline. Our proposed model matches the best performance on the *Highway* dataset and provides significantly higher performance than the other on the more challenging *Hall* benchmark. Visual inspection of the results show RKCA is the only method that doesn't fully capture the immobile people in the background, and therefore achieves the best trade-off between foreground detection and background-foreground contamination.

Algorithm	Highway	Hall
RKCA (proposed)	0.94	0.88
TRPCA '16	0.94	0.86
NC TRPCA	0.93	0.86
RPCA (baseline)	0.94	0.85
RNNLD (baseline)	0.94	0.85
HORPCA-S	0.93	0.86
Cauchy ST	0.83	0.76
Welsh ST	0.82	0.71
TRPCA '14	0.76	0.61

TABLE 2: AUC on *Highway* and *Hall* ordered by mean AUC.

7.3 Image denoising

Many natural and artificial images exhibit an inherent low-rank structure and are suitably denoised by low-rank modeling algorithms. In this section, we assess the performance of the cohort on two datasets chosen for their popularity, and for the typical use cases they represent.

We consider collections of grayscale images, and color images represented as 3-way tensors. Laplacian (salt &

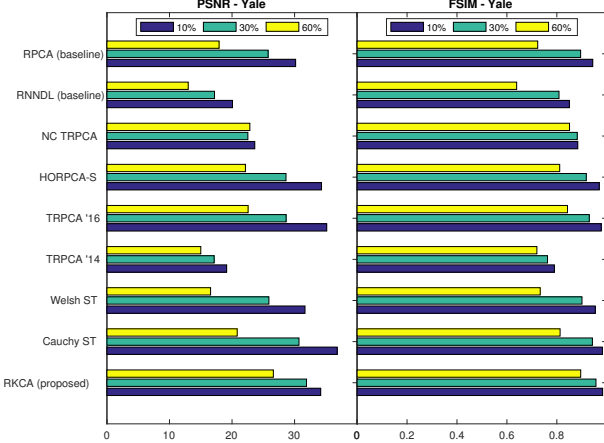


Fig. 6: Mean PSNR and FSIM on the 64 images of the first subject of *Yale* at noise levels 10%, 30%, and 60%.

pepper) noise was introduced separately in all frontal slices of the observation tensor at three different levels: 10%, 30%, and 60%, to simulate medium, high, and gross corruption. In these experiments we set the value of α to 1×10^{-3} for noise levels up to 30%, and to 1×10^{-2} at the 60% level.

We report two quantitative metrics designed to measure two key aspects of image recovery. The *Peak Signal To Noise Ratio (PSNR)* will be used as an indicator of the element-wise reconstruction quality of the signals, while the *Feature Similarity Index (FSIM, FSIMc for color images)* [49] evaluates the recovery of structural information. Quantitative metrics are not perfect replacements for subjective visual assessment of image quality; therefore, we present sample reconstructed images for verification. Our measure of choice for determining which images to compare visually is the FSIM(c) for its higher correlation with human evaluation than the PSNR.

7.3.1 Monochromatic face images

Our face denoising experiment uses the Extended Yale-B dataset [50] of 10 different subjects, each under 64 different lighting conditions. According to [51], [52], face images of one subject under various illuminations lie approximately on a 9-dimensional subspace, and are therefore suitable for low-rank modeling. We used the pre-cropped 64 images of the first subject and kept them at full resolution. The resulting collection of images constitutes a 3-way tensor of 64 images of size 192×168 . Each mode corresponds respectively to the columns and rows of the images, and to the illumination component. All three are expected to be low-rank due to the spatial correlation within frontal slices and to the correlation between images of the same subject under different illuminations. We present the comparative quantitative performance of the methods tested in Figure 6, and provide visualizations of the reconstructed first image at the 30% noise level in Figure 7. We report the metrics averaged on the 64 images.

At the 10% noise level, nearly every method provided good to excellent recovery of the original images. We therefore omit this noise level (cf. Appendix E). On the other hand, most methods, with the notable exception of RKCA, NC TRPCA, and TRPCA '16, failed to provide acceptable reconstruction in the gross corruption case. Thus, we present

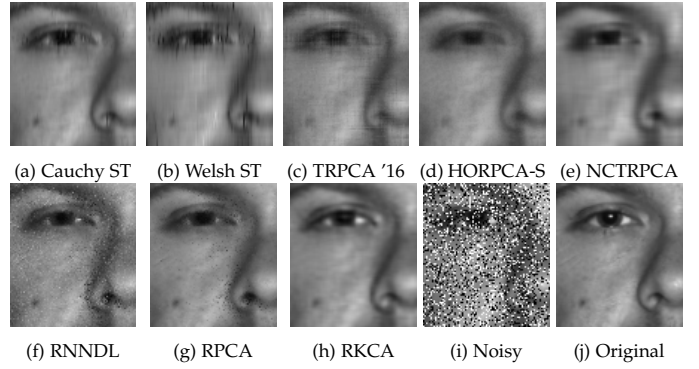


Fig. 7: Results on the *Yale* benchmark with 30% noise. TRPCA '14 removed.

the denoised images at the 30% level, and compare the performance of the three best performing methods in Table 3 for the 60% noise level.

Clear differences appeared at the 30% noise level, as demonstrated both by the quantitative metrics, and by visual inspection of Figure 7. Overall, performance was markedly lower than at the 10% level, and most methods started to lose much of the details. Visual inspection of the results confirms a higher reconstruction quality for RKCA. We invite the reader to look at the texture of the skin, the white of the eye, and at the reflection of the light on the subject's skin and pupil. The latter, in particular, is very close in nature to the white pixel corruption of the salt & pepper noise. Out of all methods, RKCA provided the best reconstruction quality: it is the only algorithm that removed all the noise and for which all the aforementioned details are distinguishable in the reconstruction.

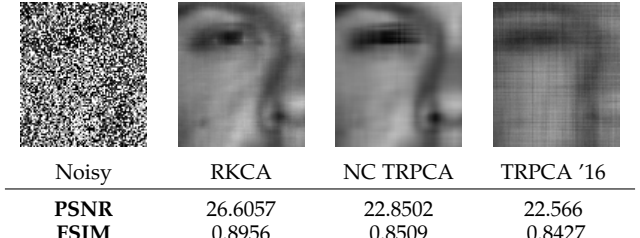


TABLE 3: Three best results on *Yale* at 60% noise.

At the 60% noise level, our method scored markedly higher than its competitors on image quality metrics, as seen both in Figure 6 and in Table 3. Visualizing the reconstructions confirms the difference: the image recovered by RKCA at the 60% noise level is comparable to the output of competing algorithms at the 30% noise level.

7.3.2 Color image denoising

Our benchmark is the *Facade* image [53]: the rich details and lighting makes it interesting to assess fine reconstruction. The geometric nature of the building's front wall, and the strong correlation between the RGB bands indicate the data can be modeled by a low-rank 3-way tensor where each frontal slice is a color channel.

At the 10% noise level, RKCA attained the highest PSNR, and among the highest FSIMc values. Most methods provided excellent reconstruction, in agreement with the high

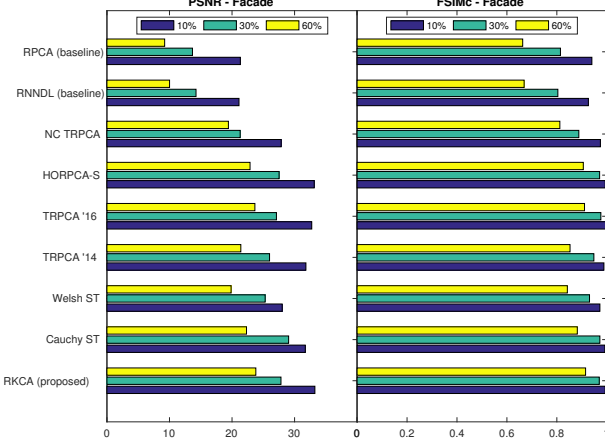


Fig. 8: PSNR and FSIMc of all methods on the Facade benchmark at noise levels 10%, 30%, and 60%.

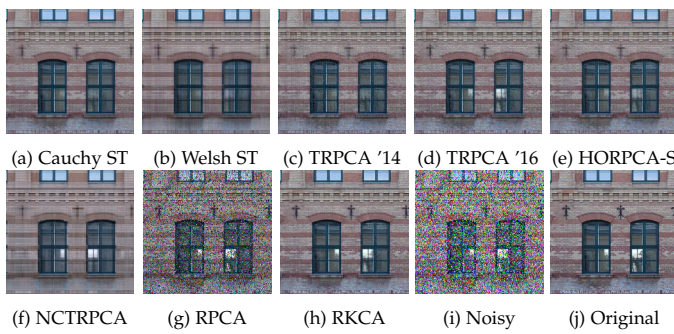


Fig. 9: Results on the Facade benchmark with 30% noise.

values of the metrics shown in Figure 8. As in the previous benchmark, the results are in Appendix E. At the 30% noise level, Cauchy ST exhibited the highest PSNR, while TRPCA '16 scored best on the FSIMc metric. RKCA had the second highest PSNR and among the highest FSIMc scores. Details are provided in Figure 23. Clear differences are visible, and are best seen on the fine details of the picture, such as the black iron ornaments, or the light coming through the window. Our method best preserved the dynamics of the lighting, and the sharpness of the details, and in the end provided the reconstruction visually closest to the original. Competing models tend to oversmooth the image, and to make the light dimmer; indicating substantial losses of high-frequency and dynamic information. RKCA appears to also provide the best color fidelity.

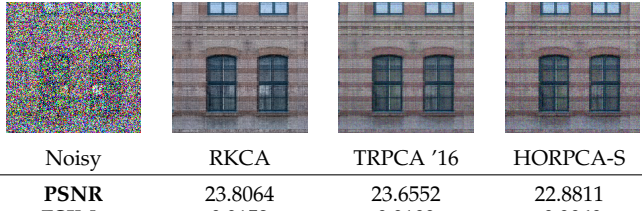


TABLE 4: Three best results on *Facade* at 60% noise.

In the gross-corruption case, RKCA was the only method with TRPCA '16 and HORPCA-S to provide a reconstruction with distinguishable details, and did it best (Figure 4).

7.4 Tensor completion

To showcase the tensor completion capabilities of our algorithm, we implemented an LADMM method to solve problem (21) with $f(\mathcal{L}) = \alpha \|\mathcal{R}\|_1 + \frac{1}{2}(\|\mathbf{A}\|_F^2 + \|\mathbf{B}\|_F^2)$. We provide comparison with one robust tensor completion model (HORPCA-S with missing values [7]) and the matrix Robust PCA with missing values [11].

7.4.1 Yale-B with noise and missing values

Our first experiment extends Section 7.3.1: we investigate the case where apart from corruption, some values are missing. We generated the data by first introducing 30% salt & pepper noise, then removing 30% of the pixels at random.

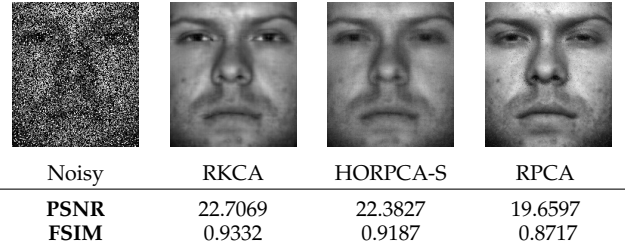


TABLE 5: Reconstruction of the first face of Yale-B with 30% salt & pepper noise and 30% missing values.

As seen in Table 5, RKCA markedly outperformed both other models in terms of FSIM, which translates into a more natural reconstruction. HORPCA-S achieved a similar PSNR but many details are lost, while RPCA removed much of the image's details and left some corruption.

7.4.2 300 Faces in the Wild

Our second experiment is on the completion of unwarped 3D faces with partial self-occlusions taken from the 300 faces in the wild challenge [54], [55], [56].

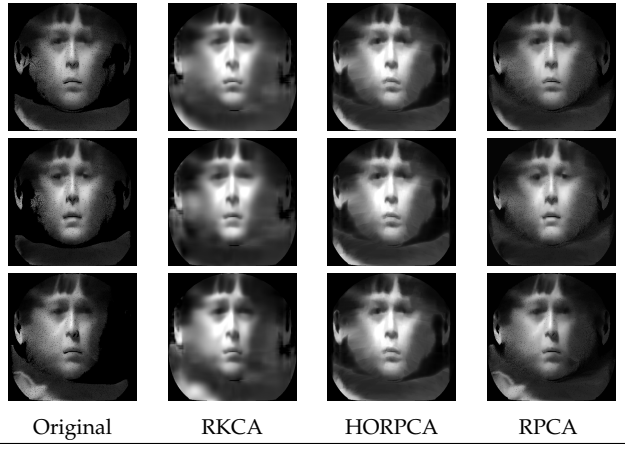


TABLE 6: Completion experiment on the 300W dataset.

We present in Table 6 the occluded frames 1, 44, and 76 of a video of the dataset, and the completed frames obtained with RKCA, HORPCA-S, and RPCA. Since no corruption is present in the dataset, the λ parameters were fixed to a high value (1×10^4) such that the algorithms behaved as tensor or matrix completion models. For RKCA, we bounded the rank of the reconstruction to 50 and performed grid-search on 5 values of the α parameter.

It is clear from Table 6 that RKCA provides the most completion. HORPCA-S is able to complete sparse missing values at the center of the image but misses out on the self-occlusions at the right. Matrix RPCA failed to complete the frames on this benchmark.

8 CONCLUSION

In this work we presented RKCA, a framework for robust low-rank representation learning on separable dictionaries that expresses the problem as a tensor factorization. We proposed three different regularizers and derived the steps for both ADMM and LADMM solvers. We showed the factorization assumed can be expressed in an equivalent way that gives optimality guarantees when coupled with a regularizer that is positively-homogeneous of degree 3. We then further discussed the low-rank properties of the models, and their practical implementation. We reached the conclusion that our model with a degree 2 regularizer, achieved a good trade-off between experimental effectiveness and parameter tuning difficulty.

Future work can seek to develop a supervised variant of RKCA that could be applied to the same tasks. Another extension that we leave for future work is to consider non-convex regularizers: it is well-known that letting $p \rightarrow 0$ in the element-wise ℓ_p and in the Scatten- p norms recover respectively the ℓ_0 pseudo-norm and the rank functions. We refer to [57] for an example in the matrix RPCA case.

ACKNOWLEDGMENTS

Mehdi Bahri was partially funded by the Department of Computing, Imperial College London. The work of Y. Panagakis has been partially supported by the European Community Horizon 2020 [H2020/2014-2020] under Grant Agreement No. 645094 (SEWA). S. Zafeiriou was partially funded by EPSRC Project EP/N007743/1 (FACER2VM).

REFERENCES

- [1] K. Pearson, "On Lines and Planes of Closest Fit to Systems of Points in Space," *Philosophical Magazine*, vol. 2, no. 6, pp. 559–572, 1901.
- [2] H. Hotelling, "Analysis of a complex of statistical variables into principal components," *Journal of Educational Psychology*, vol. 24, no. 6, pp. 417–441, 1933.
- [3] Y. LeCun, B. Boser, J. S. Denker, D. Henderson, R. E. Howard, W. Hubbard, and L. D. Jackel, "Backpropagation Applied to Handwritten Zip Code Recognition," *Neural Computation*, vol. 1, no. 4, pp. 541–551, 1989.
- [4] Y. LeCun, L. Bottou, Y. Bengio, and P. Haffner, "Gradient Based Learning Applied to Document Recognition," *Proceedings of the IEEE*, vol. 86, no. 11, pp. 2278–2324, 1998.
- [5] Y. Lecun, Y. Bengio, and G. Hinton, "Deep learning," *Nature*, vol. 521, no. 7553, pp. 436–444, 2015.
- [6] N. Xue, G. Papamakarios, M. Bahri, Y. Panagakis, and S. Zafeiriou, "Robust Low-rank Tensor Modelling Using Tucker and CP Decomposition," in *25th European Signal Processing Conference (EUSIPCO 2017), special session on Component Analysis for Computer Vision*, 2017.
- [7] D. Goldfarb and Z. T. Qin, "Robust Low-Rank Tensor Recovery: Models and Algorithms," *SIAM Journal on Matrix Analysis and Applications*, vol. 35, no. 1, pp. 225–253, mar 2014.
- [8] R. Rubinstein, A. M. Bruckstein, and M. Elad, "Dictionaries for sparse representation modeling," *Proceedings of the IEEE*, vol. 98, no. 6, pp. 1045–1057, jun 2010.
- [9] B. A. Olshausen and D. J. Field, "Sparse coding with an overcomplete basis set: A strategy employed by V1?" *Vision Research*, vol. 37, no. 23, pp. 3311–3325, 1997.
- [10] H. Zou, T. Hastie, and R. Tibshirani, "Sparse principal component analysis," *Journal of Computational and Graphical Statistics*, vol. 15, no. 2, pp. 265–286, 2006.
- [11] E. J. Candès, X. Li, Y. Ma, and J. Wright, "Robust principal component analysis?" *Journal of the ACM*, vol. 58, no. 3, pp. 1–37, may 2011.
- [12] J. Wright, Y. Ma, J. Mairal, G. Sapiro, T. S. Huang, and S. Yan, "Sparse Representation for Computer Vision and Pattern Recognition," *Proceedings of the IEEE*, vol. 98, no. 6, pp. 1031–1044, jun 2010.
- [13] M. Aharon, M. Elad, and A. Bruckstein, "K-SVD: An algorithm for designing overcomplete dictionaries for sparse representation," *IEEE Transactions on Signal Processing*, vol. 54, no. 11, pp. 4311–4322, 2006.
- [14] J. Mairal, M. Elad, and G. Sapiro, "Sparse learned representations for image restoration," *Sparse learned representations for image restoration*, no. December, pp. 1–10, 2008.
- [15] S. Hawe, M. Seibert, and M. Kleinstuber, "Separable Dictionary Learning," *Proceedings of the IEEE Computer Society Conference on Computer Vision and Pattern Recognition*, mar 2013.
- [16] S. H. Hsieh, C. S. Lu, and S. C. Pei, "2D sparse dictionary learning via tensor decomposition," *2014 IEEE Global Conference on Signal and Information Processing, GlobalSIP 2014*, pp. 492–496, 2014.
- [17] Y. Fang, J. Wu, and B. Huang, "2D sparse signal recovery via 2D orthogonal matching pursuit," *Science China Information Sciences*, vol. 55, no. 4, pp. 889–897, 2012.
- [18] R. a. Harshman, "Foundations of the PARAFAC procedure: Models and conditions for an explanatory multimodal factor analysis," *UCLA Working Papers in Phonetics*, vol. 16, no. 10, pp. 1–84, 1970.
- [19] J. D. Carroll and J.-J. Chang, "Analysis of individual differences in multidimensional scaling via an n-way generalization of "Eckart-Young" decomposition," *Psychometrika*, vol. 35, no. 3, pp. 283–319, 1970.
- [20] S. Boyd, "Distributed Optimization and Statistical Learning via the Alternating Direction Method of Multipliers," *Foundations and Trends® in Machine Learning*, vol. 3, no. 1, pp. 1–122, 2010.
- [21] M. Bahri, Y. Panagakis, and S. Zafeiriou, "Robust kronecker-decomposable component analysis for low-rank modeling," in *The IEEE International Conference on Computer Vision (ICCV)*, Oct 2017.
- [22] B. Haeffele, E. Young, and R. Vidal, "Structured low-rank matrix factorization: Optimality, algorithm, and applications to image processing," in *Proceedings of the 31st International Conference on Machine Learning (ICML-14)*, T. Jebara and E. P. Xing, Eds. JMLR Workshop and Conference Proceedings, 2014, pp. 2007–2015.
- [23] B. D. Haeffele and R. Vidal, "Global Optimality in Tensor Factorization, Deep Learning, and Beyond," *CoRR*, vol. abs/1506.0, 2015.
- [24] Z. Zhang, G. Ely, S. Aeron, N. Hao, and M. Kilmer, "Novel methods for multilinear data completion and de-noising based on tensor-SVD," *Proceedings of the IEEE Computer Society Conference on Computer Vision and Pattern Recognition*, pp. 3842–3849, 2014.
- [25] C. Lu, J. Feng, Y. Chen, W. Liu, Z. Lin, and S. Yan, "Tensor Robust Principal Component Analysis: Exact Recovery of Corrupted Low-Rank Tensors via Convex Optimization," in *The IEEE Conference on Computer Vision and Pattern Recognition (CVPR)*, 2016.
- [26] T. G. Kolda and B. W. Bader, "Tensor Decompositions and Applications," *SIAM Review*, vol. 51, no. 3, pp. 455–500, aug 2009.
- [27] B. Recht, M. Fazel, and P. A. Parrilo, "Guaranteed Minimum-Rank Solutions of Linear Matrix Equations via Nuclear Norm Minimization," *Optimization Online*, vol. 52, no. 3, pp. 1–33, jun 2007.
- [28] G. Golub, S. Nash, and C. Van Loan, "A Hessenberg-Schur method for the problem $AX + XB = C$," *IEEE Transactions on Automatic Control*, vol. 24, no. 6, pp. 909–913, dec 1979.
- [29] F. Shang, Y. Liu, J. Cheng, and H. Cheng, "Robust Principal Component Analysis with Missing Data," *Proceedings of the 23rd ACM International Conference on Conference on Information and Knowledge Management - CIKM '14*, no. 1, pp. 1149–1158, 2014.
- [30] X. Peng, C. Lu, Z. Yi, and H. Tang, "Connections Between Nuclear-Norm and Frobenius-Norm-Based Representations," *Tnnls*, no. 2, pp. 1–7, 2016.
- [31] G. Liu, Z. Lin, S. Yan, J. Sun, Y. Yu, and Y. Ma, "Robust recovery of subspace structures by low-rank representation," *IEEE Trans. Pattern Anal. Mach. Intell.*, vol. 35, no. 1, pp. 171–184, Jan. 2013.

[32] H. Zhang, Z. Yi, and X. Peng, "FLRR: Fast low-rank representation using Frobenius-norm," *Electronics Letters*, vol. 50, no. 13, pp. 936–938, 2014.

[33] T. F. Chan, "An Improved Algorithm for Computing the Singular Value Decomposition," *ACM Transactions on Mathematical Software*, vol. 8, no. 1, pp. 72–83, 1982.

[34] J. Dean and S. Ghemawat, "MapReduce: Simplified Data Processing on Large Clusters," *Proceedings of 6th Symposium on Operating Systems Design and Implementation*, pp. 137–149, 2004.

[35] Z. Lin, R. Liu, and Z. Su, "Linearized alternating direction method with adaptive penalty for low-rank representation," vol. 2, article 6, 09 2011.

[36] Z. Xu, M. A. T. Figueiredo, and T. Goldstein, "Adaptive ADMM with Spectral Penalty Parameter Selection," vol. 2, no. 2, 2016.

[37] Y. Xu, M. Liu, Q. Lin, and T. Yang, "ADMM without a Fixed Penalty Parameter: Faster Convergence with New Adaptive Penalization," no. 1, pp. 1–11, 2017.

[38] M. Hong, Z. Q. Luo, and M. Razaviyayn, "Convergence analysis of alternating direction method of multipliers for a family of nonconvex problems," in *2015 IEEE International Conference on Acoustics, Speech and Signal Processing (ICASSP)*, April 2015, pp. 3836–3840.

[39] Y. Wang, W. Yin, and J. Zeng, "Global Convergence of ADMM in Nonconvex Nonsmooth Optimization," *ArXiv e-prints*, Nov. 2015.

[40] Z. Lin, M. Chen, and Y. Ma, "The Augmented Lagrange Multiplier Method for Exact Recovery of Corrupted Low-Rank Matrices," *arXiv:1009.5055*, p. 23, sep 2010.

[41] Q. Pan, D. Kong, C. Ding, and B. Luo, "Robust non-negative dictionary learning," in *Proceedings of the Twenty-Eighth AAAI Conference on Artificial Intelligence*, ser. AAAI'14. AAAI Press, 2014, pp. 2027–2033.

[42] Y. Yang, Y. Feng, and J. A. K. Suykens, "Robust Low-Rank Tensor Recovery With Regularized Redescending M-Estimator," *IEEE Transactions on Neural Networks and Learning Systems*, vol. 27, no. 9, pp. 1933–1946, sep 2015.

[43] A. Anandkumar, P. Jain, Y. Shi, and U. N. Niranjan, "Tensor vs Matrix Methods: Robust Tensor Decomposition under Block Sparse Perturbations," in *Proceedings of the 19th International Conference on Artificial Intelligence and Statistics, AISTATS 2016*, A. Gretton and R. C. Christian, Eds. Cadiz, Spain: JMLR.org, 2016.

[44] P. Netrapalli, U. N. Niranjan, S. Sanghavi, A. Anandkumar, and P. Jain, "Non-convex Robust PCA," *Advances in Neural Information Processing Systems 27 (Proceedings of NIPS)*, pp. 1–9, oct 2014.

[45] N. Goyette, P. M. Jodoin, F. Porikli, J. Konrad, and P. Ishwar, "changedetection.net: A new change detection benchmark dataset," in *IEEE Computer Society Conference on Computer Vision and Pattern Recognition Workshops*, 2012, pp. 1–8.

[46] L. Li, W. Huang, I.-H. Gu, and Q. Tian, "Statistical Modeling of Complex Backgrounds for Foreground Object Detection," *IEEE Transactions on Image Processing*, vol. 13, no. 11, pp. 1459–1472, nov 2004.

[47] Q. Zhao, G. Zhou, L. Zhang, A. Cichocki, and S.-I. Amari, "Bayesian Robust Tensor Factorization for Incomplete Multiway Data," *IEEE Transactions on Neural Networks and Learning Systems*, vol. 27, no. 4, pp. 736–748, apr 2016.

[48] T. Fawcett, "An introduction to ROC analysis," *Pattern Recognition Letters*, vol. 27, no. 8, pp. 861–874, 2006.

[49] Lin Zhang, Lei Zhang, Xuanqin Mou, and D. Zhang, "FSIM: A Feature Similarity Index for Image Quality Assessment," *IEEE Transactions on Image Processing*, vol. 20, no. 8, pp. 2378–2386, aug 2011.

[50] A. Georghiades, P. Belhumeur, and D. Kriegman, "From few to many: illumination cone models for face recognition under variable lighting and pose," *IEEE Transactions on Pattern Analysis and Machine Intelligence*, vol. 23, no. 6, pp. 643–660, jun 2001.

[51] R. Ramamoorthi and P. Hanrahan, "An efficient representation for irradiance environment maps," in *Proceedings of the 28th annual conference on Computer graphics and interactive techniques - SIGGRAPH '01*, vol. 64, no. 1. New York, New York, USA: ACM Press, 2001, pp. 497–500.

[52] R. Basri and D. Jacobs, "Lambertian reflectance and linear subspaces," *IEEE Transactions on Pattern Analysis and Machine Intelligence*, vol. 25, no. 2, pp. 218–233, feb 2003.

[53] X. Chen, Z. Han, Y. Wang, Q. Zhao, D. Meng, and Y. Tang, "Robust Tensor Factorization with Unknown Noise," in *The IEEE Conference on Computer Vision and Pattern Recognition (CVPR)*, 2016, pp. 5213–5221.

[54] C. Sagonas, G. Tzimiropoulos, S. Zafeiriou, and M. Pantic, "300 faces in-the-wild challenge: The first facial landmark Localization Challenge," *Proceedings of the IEEE International Conference on Computer Vision*, pp. 397–403, 2013.

[55] —, "A semi-automatic methodology for facial landmark annotation," *IEEE Computer Society Conference on Computer Vision and Pattern Recognition Workshops*, pp. 896–903, 2013.

[56] C. Sagonas, E. Antonakos, G. Tzimiropoulos, S. Zafeiriou, and M. Pantic, "300 Faces In-The-Wild Challenge: database and results," *Image and Vision Computing*, vol. 47, pp. 3–18, 2015.

[57] G. Papamakarios, Y. Panagakis, and S. Zafeiriou, "Generalised scalable robust principal component analysis," in *Proceedings of the British Machine Vision Conference*, 2014.

[58] A. Laub, *Matrix Analysis for Scientists and Engineers*. Society for Industrial and Applied Mathematics, 2005.



Mehdi Bahri is a PhD student with Stefanos Zafeiriou at the Department of Computing, Imperial College London. He received his Diplôme d'Ingénieur in Applied Mathematics with Honours from Grenoble Institute of Technology - Ensimeg and an MSc in Advanced Computing with Distinction from Imperial College London, both in 2016. He published his master's research in ICCV and spent one year in the industry. His research interests include representation learning, geometric deep learning, and Bayesian learning.



Yannis Panagakis is a Research Fellow in the Department of Computing, Imperial College London and a Lecturer with Middlesex University London. He received his PhD and MSc degrees from the Department of Informatics, Aristotle University of Thessaloniki and his B.Sc. degree in Informatics and Telecommunication from the National and Kapodistrian University of Athens, Greece. Yannis received various scholarships and awards for his studies and research, including the prestigious Marie-Curie Fellowship in 2013. His current research interests include machine learning, signal processing, and mathematical optimization with applications to computer vision, human behaviour analysis, and music information research.



Stefanos Zafeiriou is currently a Reader in Pattern Recognition/Statistical Machine Learning for Computer Vision with the Department of Computing, Imperial College London, London, U.K., and a Distinguishing Research Fellow with University of Oulu under Finish Distinguishing Professor Programme. He was a recipient of the Prestigious Junior Research Fellowships from Imperial College London in 2011 to start his own independent research group. He was the recipient of the Presidents Medal for Excellence in Research Supervision for 2016. He has received various awards during his doctoral and post-doctoral studies. He currently serves as an Associate Editor of the IEEE Transactions on Cybernetics the Image and Vision Computing Journal. He has been a Guest Editor of over six journal special issues and co-organised over nine workshops/special sessions on face analysis topics in top venues, such as CVPR/FG/ICCV/ECCV (including two very successfully challenges run in ICCV13 and ICCV15 on facial landmark localisation/tracking). He has more than 5000 citations to his work, h-index 37. He is the General Chair of BMVC 2017.

APPENDIX A

PROXIMAL OPERATORS

A.1 Selective shrinkage operator

We prove the result for a general D -dimensional tensor \mathcal{X} .

Proof. The proximal operator of $\|\pi_\Omega(\cdot)\|_1$ satisfies:

$$P_{\|\pi_\Omega(\cdot)\|_1}(\mathcal{X}) = \operatorname{argmin}_{\mathcal{Y}} \|\pi_\Omega(\mathcal{Y})\|_1 + \frac{1}{2} \|\mathcal{X} - \mathcal{Y}\|_F^2 \quad (56)$$

By direct case analysis, if $i = (i_1, i_2, \dots, i_N) \in \Omega$:

$$(P_{\|\pi_\Omega(\cdot)\|_1})_i = \operatorname{argmin}_{\mathcal{Y}_i} \|\mathcal{Y}_i\|_1 + \frac{1}{2} \|\mathcal{X}_i - \mathcal{Y}_i\|_F^2 \quad (57)$$

Which is the expression of the standard shrinkage operator $\mathcal{S}(\mathcal{X}_i)$. If $i \in \bar{\Omega}$, then:

$$(P_{\|\pi_\Omega(\cdot)\|_1})_i = \operatorname{argmin}_{\mathcal{Y}_i} \frac{1}{2} \|\mathcal{X}_i - \mathcal{Y}_i\|_F^2 = \mathcal{X}_i \quad (58)$$

□

A.2 Schatten- p norms

Proposition A.1. Let $\mathbf{A} \in \mathbb{R}^{m \times n}$ and $p > 0$, denote by $\|\cdot\|_p$ the Schatten- p norm and the ℓ_p norm, and by $\operatorname{diag}(\cdot)$ the operator define by:

- $\operatorname{diag}(\mathbf{X})$ is the main diagonal of the matrix \mathbf{X}
- $\operatorname{diag}(\mathbf{X})$ is the square matrix with the vector x as main diagonal

Then if $\mathbf{A} = \mathbf{U}\Sigma\mathbf{V}^\top$ the SVD of \mathbf{A}

$$\operatorname{prox}_{\lambda\|\cdot\|_p}(\mathbf{A}) = \mathbf{U} \operatorname{diag}(\operatorname{prox}_{\lambda\|\cdot\|_p}(\operatorname{diag}(\Sigma))) \mathbf{V}^\top \quad (59)$$

APPENDIX B

UPDATING THE BASES BY SUBSTITUTION

In the case of the degree three regularizers, we can use the substitution method to tackle the non-smoothness of the Frobenius norm and of the Nuclear norm, regardless of the method used for the core tensor \mathcal{R} . We present below the derivation of the corresponding updates.

Let us introduce the auxiliary variables \mathbf{U} and \mathbf{V} for \mathbf{A} and \mathbf{B} respectively. The constrained problem becomes

$$\begin{aligned} \min_{\mathbf{A}, \mathbf{B}, \mathbf{U}, \mathbf{V}, \mathcal{K}, \mathcal{R}, \mathcal{E}} \quad & \lambda \|\mathcal{R}\|_1 \|\mathbf{B}\|_F \|\mathbf{A}\|_F + \lambda \|\mathcal{E}\|_1 \\ \text{s.t.} \quad & \mathcal{X} = \mathcal{K} \times_1 \mathbf{U} \times_2 \mathbf{V} + \mathcal{E} \\ & \mathcal{R} = \mathcal{K} \\ & \mathbf{A} = \mathbf{U} \\ & \mathbf{B} = \mathbf{V} \end{aligned} \quad (60)$$

And the Augmented Lagrangian can easily be formulated by introducing the Lagrange multipliers and the penalty parameters \mathbf{Y}_U , \mathbf{Y}_V , μ_U , and μ_V .

We present the derivations for \mathbf{A} only as the ones for \mathbf{B} are easily found by substituting the correct variables.

We have

$$\mathbf{A}^* = \operatorname{argmin}_{\mathbf{A}} [\alpha \|\mathbf{B}\|_F \|\mathcal{R}\|_1] \|\mathbf{A}\|_F + \langle \mathbf{Y}_U, \mathbf{A} - \mathbf{U} \rangle + \frac{\mu_U}{2} \|\mathbf{A} - \mathbf{U}\|_F^2 \quad (61)$$

$$= \operatorname{argmin}_{\mathbf{A}} \left[\frac{\alpha}{\mu_U} \|\mathbf{B}\|_F \|\mathcal{R}\|_1 \right] \|\mathbf{A}\|_F + \frac{1}{2} \|\mathbf{U} - \frac{1}{\mu_U} \mathbf{Y}_U - \mathbf{A}\|_F^2 \quad (62)$$

$$= \operatorname{prox}_{\frac{\alpha}{\mu_U} \|\mathbf{B}\|_F \|\mathcal{R}\|_1 \cdot \cdot \cdot} (\mathbf{U} - \frac{1}{\mu_U} \mathbf{Y}_U) \quad (63)$$

The update of \mathbf{U} is obtained by derivation

$$\begin{aligned} \mathbf{U}^* = \operatorname{argmin}_{\mathbf{U}} \frac{\mu}{2} \sum_i \|\mathbf{X}_i - \mathbf{U} \mathbf{K}_i \mathbf{V}^\top - \mathbf{E}_i\|_F^2 + \\ \sum_i \langle \mathbf{A}_i, \mathbf{X}_i - \mathbf{U} \mathbf{K}_i \mathbf{V}^\top - \mathbf{E}_i \rangle + \frac{\mu_U}{2} \|\mathbf{A} - \mathbf{U}\|_F^2 + \langle \mathbf{Y}_U, \mathbf{A} - \mathbf{U} \rangle \end{aligned} \quad (64)$$

Taking the derivative with respect to \mathbf{U} and setting to 0 we find the Sylvester's equation for \mathbf{U}^*

$$\begin{aligned} \mathbf{U}^* \left(-\frac{\mu}{\mu_U} \sum_i \mathbf{K}_i \mathbf{V}^\top \mathbf{V} \mathbf{K}_i^\top \right) - \mathbf{U}^* + \\ \frac{1}{\mu_U} \left[\mu_U \mathbf{A} + \mathbf{Y}_U + \mu \sum_i (\mathbf{X}_i - \mathbf{E}_i + \frac{1}{\mu} \mathbf{A}_i) \mathbf{V} \mathbf{K}_i^\top \right] = 0 \end{aligned} \quad (65)$$

APPENDIX C

DERIVATIONS OF THE LADMM UPDATES

This appendix contains the derivations of the Lipschitz constants of the gradients in solving the sub-problems for the LADMM algorithm of Section 4.

C.1 Overview

We briefly remind the reader of the linearization method. Provided an unconstrained optimization problem:

$$\min_{\mathbf{x}} f(\mathbf{x}) + g(\mathbf{x}) \quad (66)$$

Where f is smooth and g is non-smooth and $\mathbf{x} \in \mathbb{R}^d$. We replace f by the following quadratic approximation around \mathbf{y} :

$$q_l(\mathbf{x}, \mathbf{y}) = f(\mathbf{y}) + \langle \nabla f(\mathbf{y}), \mathbf{y} - \mathbf{x} \rangle + \frac{l}{2} \|\mathbf{y} - \mathbf{x}\|_2^2 \quad (67)$$

When ∇f is Lipschitz continuous with Lipschitz constant L and $l \geq L$ the quadratic approximation is an upper bound of f . If g has proximal operator $\operatorname{prox}_g(\cdot)$ then:

$$g(\mathbf{x}) + q_l(\mathbf{x}, \mathbf{y}) \quad (68)$$

$$= g(\mathbf{y}) + f(\mathbf{y}) + \langle \nabla f(\mathbf{y}), \mathbf{y} - \mathbf{x} \rangle + \frac{l}{2} \|\mathbf{y} - \mathbf{x}\|_2^2 \quad (69)$$

$$= g(\mathbf{y}) + \frac{l}{2} \|\mathbf{x} - \left(\mathbf{y} - \frac{1}{l} \nabla f(\mathbf{y}) \right)\|_2^2 + f(\mathbf{y}) \quad (70)$$

And $\operatorname{argmin}_{\mathbf{x}} g(\mathbf{x}) + q_l(\mathbf{x}, \mathbf{y}) = \operatorname{prox}_g(\mathbf{y} - \frac{1}{l} \nabla f(\mathbf{y}))$. In an iterative algorithm, we choose $\mathbf{x} = \mathbf{x}_{k+1}$ and $\mathbf{y} = \mathbf{x}_k$.

We start from the augmented Lagrangian of problem (40) with no auxiliary variables:

$$\begin{aligned} \mathcal{L}(\mathbf{A}, \mathbf{B}, \mathcal{R}, \mathcal{E}, \mathbf{\Lambda}, \mu) = \alpha \|\mathbf{A}\|_F \|\mathbf{B}\|_F \|\mathcal{R}\|_1 + \\ \lambda \|\mathcal{E}\|_1 + \langle \mathbf{\Lambda}, \mathcal{X} - \mathcal{R} \times_1 \mathbf{A} \times_2 \mathbf{B} - \mathcal{E} \rangle + \\ \frac{\mu}{2} \|\mathcal{X} - \mathcal{R} \times_1 \mathbf{A} \times_2 \mathbf{B} - \mathcal{E}\|_F^2 \end{aligned} \quad (71)$$

C.2 For \mathcal{R}

Let $\mathbf{\Delta} = \mathcal{X} - \mathcal{E} + \frac{1}{\mu} \mathbf{\Lambda}$ and $\mathbf{\delta} = \operatorname{vec}(\mathbf{\Delta})$, $\mathbf{r} = \operatorname{vec}(\mathcal{R})$. From the properties of the Kronecker product, $\operatorname{vec}(\mathcal{R} \times_1 \mathbf{A} \times_2 \mathbf{B}) = (\mathbf{I}_N \otimes \mathbf{B} \otimes \mathbf{A}) \operatorname{vec}(\mathbf{r})$. For the sake of brevity we let

$\Gamma = \mathbf{I}_N \otimes \mathbf{B} \otimes \mathbf{A}$. Thanks to the separability of the ℓ_1 -norm penalty, using these notations (85) is equivalent to the following vector minimization problem:

$$\min_{\mathbf{r}} \frac{\alpha}{\mu} \|\mathbf{A}\|_{\text{F}} \|\mathbf{B}\|_{\text{F}} \|\mathbf{r}\|_1 + \frac{1}{2} \|\mathbf{\Gamma r} - \boldsymbol{\delta}\|_2^2 \quad (72)$$

Vector calculus gives the following gradient for the quadratic part:

$$\nabla_{\mathbf{r}}(\mathbf{r}) = \frac{\partial}{\partial \mathbf{r}} \frac{1}{2} \|\mathbf{\Gamma r} - \boldsymbol{\delta}\|_2^2 = \mathbf{\Gamma}^T (\mathbf{\Gamma r} - \boldsymbol{\delta}) \quad (73)$$

The computation of the Lipschitz constant is then straightforward:

$$\|\nabla_{\mathbf{r}}(\mathbf{r}_1) - \nabla_{\mathbf{r}}(\mathbf{r}_2)\|_2 = \|\mathbf{\Gamma}^T \mathbf{\Gamma} (\mathbf{r}_1 - \mathbf{r}_2)\|_2 \quad (74)$$

$$\leq \|\|\mathbf{\Gamma}^T \mathbf{\Gamma}\| \cdot \|\mathbf{r}_1 - \mathbf{r}_2\|_2 \quad (75)$$

Where $\|\cdot\|$ denotes the induced norm, i.e., the largest singular value. We again make use of the properties of the Kronecker product to find:

$$\|\|\mathbf{\Gamma}^T \mathbf{\Gamma}\| = \|\|(\mathbf{I}_N \otimes \mathbf{B} \otimes \mathbf{A})^T (\mathbf{I}_N \otimes \mathbf{B} \otimes \mathbf{A})\| \| \quad (76)$$

$$= \|\|\mathbf{I}_N^T \mathbf{I}_N \otimes \mathbf{B}^T \mathbf{B} \otimes \mathbf{A}^T \mathbf{A}\| \| \quad (77)$$

$$= \|\|\mathbf{B}^T \mathbf{B}\| \cdot \|\mathbf{A}^T \mathbf{A}\| \| \quad (78)$$

$$= \sigma_{\max}^2(\mathbf{B}) \cdot \sigma_{\max}^2(\mathbf{A}) \quad (79)$$

In this case, we recommend direct calculation of the constant instead of using a backtracking procedure because the matrices \mathbf{A} and \mathbf{B} will often be of small size (if working on small input data or if providing a small upper bound r on the rank) and the computation can be performed by partial SVD in all cases.

Finally, going back to tensor form we find equation (44).

C.3 For \mathbf{A} and \mathbf{B}

Again we compute $\nabla_{\mathbf{A}}(\mathbf{A}) = \frac{\partial}{\partial \mathbf{A}} \frac{1}{2} \sum_i \|\mathbf{\Delta}_i - \mathbf{A} \mathbf{C}_i\|_{\text{F}}^2 = \sum_i (\mathbf{A} \mathbf{C}_i - \mathbf{\Delta}_i) \mathbf{C}_i^T$.

The Lipschitz constant is:

$$\|\nabla_{\mathbf{A}}(\mathbf{A}_1) - \nabla_{\mathbf{A}}(\mathbf{A}_2)\|_{\text{F}} \quad (80)$$

$$= \|\sum_i (\mathbf{A}_1 \mathbf{C}_i - \mathbf{\Delta}_i) \mathbf{C}_i^T - \sum_i (\mathbf{A}_2 \mathbf{C}_i - \mathbf{\Delta}_i) \mathbf{C}_i^T\|_{\text{F}} \quad (81)$$

$$= \|\sum_i (\mathbf{A}_1 - \mathbf{A}_2) \mathbf{C}_i \mathbf{C}_i^T\|_{\text{F}} \quad (82)$$

$$= \|(\mathbf{A}_1 - \mathbf{A}_2) \sum_i \mathbf{C}_i \mathbf{C}_i^T\|_{\text{F}} \quad (83)$$

$$\leq \|\mathbf{A}_1 - \mathbf{A}_2\|_{\text{F}} \|\sum_i \mathbf{C}_i \mathbf{C}_i^T\|_{\text{F}} \quad (84)$$

From the sub-multiplicativity of Schatten norms.

The sub-problem for \mathbf{B} is:

$$\begin{aligned} & \min_{\mathbf{B}} \alpha \|\mathbf{A}\|_{\text{F}} \|\mathbf{B}\|_{\text{F}} \|\mathcal{R}\|_1 + \\ & \frac{\mu}{2} \|\mathcal{X} - \mathcal{R} \times_1 \mathbf{A} \times_2 \mathbf{B} - \mathcal{E} + \frac{1}{\mu} \mathbf{\Lambda}\|_{\text{F}}^2 \end{aligned} \quad (85)$$

Using the same Δ notation from the update of \mathcal{R} and denoting $\mathbf{D}_i = \mathbf{A} \mathbf{R}_i$ we have

$$\mathbf{B}^* = \operatorname{argmin}_{\mathbf{B}} \left[\frac{\alpha}{\mu} \|\mathbf{B}\|_{\text{F}} + \frac{1}{2} \sum_i \|\mathbf{\Delta}_i - \mathbf{D}_i \mathbf{B}^T\|_{\text{F}}^2 \right] \quad (86)$$

We compute $\nabla_{\mathbf{B}}(\mathbf{B}) = \frac{\partial}{\partial \mathbf{B}} \frac{1}{2} \sum_i \|\mathbf{\Delta}_i - \mathbf{D}_i \mathbf{B}^T\|_{\text{F}}^2 = \sum_i (\mathbf{B} \mathbf{D}_i^T - \mathbf{\Delta}_i^T) \mathbf{D}_i$.

And similar to \mathbf{A} the Lipschitz constant:

$$\|\nabla_{\mathbf{B}}(\mathbf{B}_1) - \nabla_{\mathbf{B}}(\mathbf{B}_2)\|_{\text{F}} \quad (87)$$

$$= \|\sum_i (\mathbf{B}_1 \mathbf{D}_i^T - \mathbf{\Delta}_i^T) \mathbf{D}_i - \sum_i (\mathbf{B}_2 \mathbf{D}_i^T - \mathbf{\Delta}_i^T) \mathbf{D}_i\|_{\text{F}} \quad (88)$$

$$= \|\sum_i (\mathbf{B}_1 - \mathbf{B}_2) \mathbf{D}_i^T \mathbf{D}_i\|_{\text{F}} \quad (89)$$

$$= \|(\mathbf{B}_1 - \mathbf{B}_2) \sum_i \mathbf{D}_i^T \mathbf{D}_i\|_{\text{F}} \quad (90)$$

$$\leq \|\mathbf{A}_1 - \mathbf{A}_2\|_{\text{F}} \|\sum_i \mathbf{D}_i^T \mathbf{D}_i\|_{\text{F}} \quad (91)$$

APPENDIX D

SCHATTEN NORMS AND THE KRONECKER PRODUCT

In this Section we prove the identity used in Section 2.2 on the Schatten norm of a Kronecker product.

Let us first remind the reader of the definition of the Schatten- p norm:

Definition D.1. Let \mathbf{A} a real-valued matrix, $\mathbf{A} \in \mathbb{R}^{m \times n}$. The Schatten- p norm of \mathbf{A} is defined as:

$$\|\mathbf{A}\|_p = \left(\sum_i s_i^p \right)^{1/p}$$

Where s_i is the i^{th} singular value of \mathbf{A} .

We argued the result stems from the compatibility of the Kronecker product with the singular value decomposition, that is:

Proposition D.1. Let $\mathbf{A} = \mathbf{U}_A \Sigma_A \mathbf{V}_A^T$, $\mathbf{B} = \mathbf{U}_B \Sigma_B \mathbf{V}_B^T$ two real-valued matrices given by their SVD, then:

$$\mathbf{A} \otimes \mathbf{B} = (\mathbf{U}_A \otimes \mathbf{U}_B)(\Sigma_A \otimes \Sigma_B)(\mathbf{V}_A^T \otimes \mathbf{V}_B^T)$$

Proof. See [58]. \square

The identity we used is formally expressed in Theorem D.1, of which we give the proof for completeness.

Theorem D.1. Let $\mathbf{A} \in \mathbb{R}^{m \times n}$ and $\mathbf{B} \in \mathbb{R}^{p \times q}$, then:

$$\forall p > 0, \|\mathbf{A} \otimes \mathbf{B}\|_p = \|\mathbf{A}\|_p \|\mathbf{B}\|_p$$

Where $\|\cdot\|_p$ denotes the Schatten- p norm.

Proof. From Proposition 1, the singular values of $\mathbf{A} \otimes \mathbf{B}$ are the $\sigma_{A,i} \sigma_{B,j}$ so:

$$\begin{aligned} \|\mathbf{A} \otimes \mathbf{B}\|_p &= \left(\sum_{i,j} (\sigma_{A,i} \sigma_{B,j})^p \right)^{1/p} \\ &= \left(\sum_{i,j} \sigma_{A,i}^p \sigma_{B,j}^p \right)^{1/p} \\ &= \left(\sum_i \sigma_{A,i}^p \sum_j \sigma_{B,j}^p \right)^{1/p} \\ &= \left(\sum_i \sigma_{A,i}^p \right)^{1/p} \left(\sum_j \sigma_{B,j}^p \right)^{1/p} \\ &= \|\mathbf{A}\|_p \|\mathbf{B}\|_p \end{aligned}$$

\square

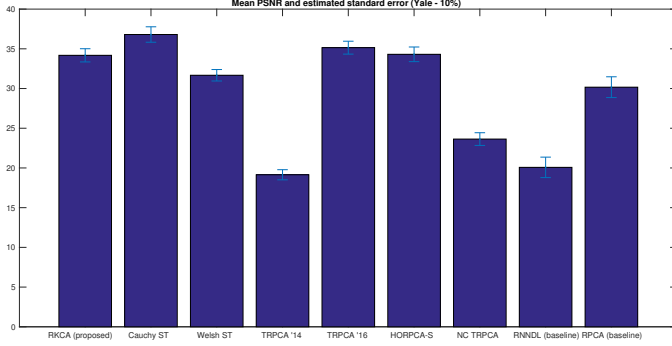


Fig. 10: Mean PSNR and standard error at the 10% noise level.

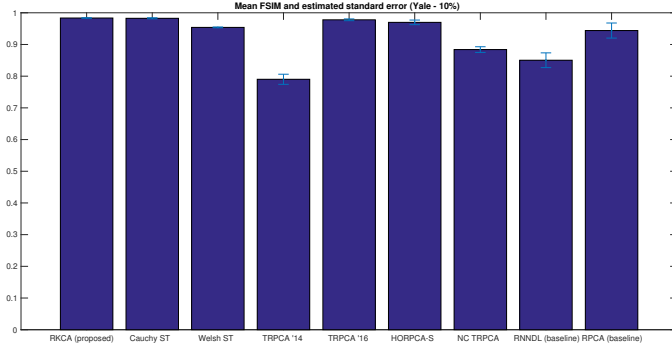


Fig. 11: Mean FSIM and standard error at the 10% noise level.

APPENDIX E ADDITIONAL EXPERIMENTAL RESULTS

In this Section we provide additional information on the results reported in the paper, as well as supporting material.

E.1 Mean performance on the Yale dataset

On the Yale-B experiment, the measurements we present are average values over the 64 images of the first subject. There is therefore an uncertainty on the measures that we wish to address here.

We present in the following figures the mean values along with their estimated standard error. The formula we used for the standard error is

$$\text{STDERR} = 1.96 \frac{\hat{s}}{\sqrt{n}}$$

With \hat{s} the sample standard deviation, and n the sample size (64).

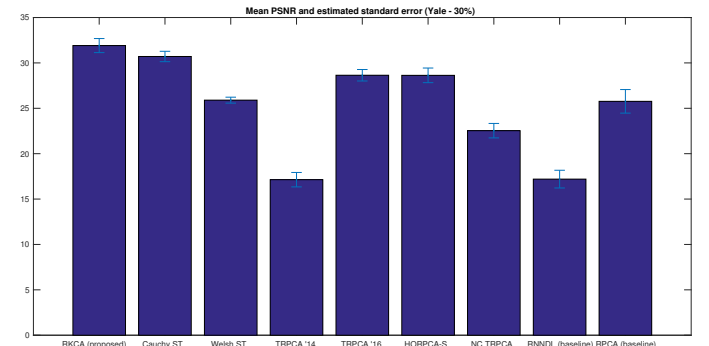


Fig. 12: Mean PSNR and standard error at the 30% noise level.

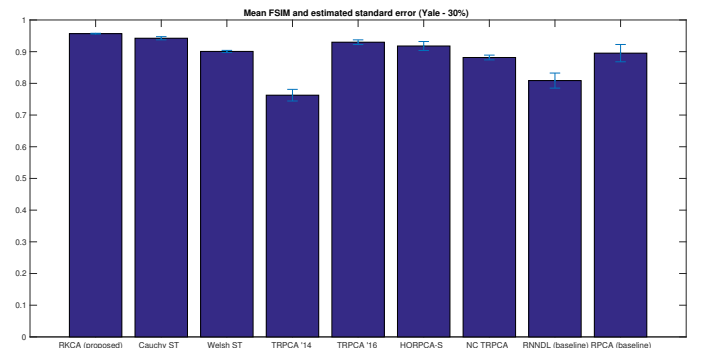


Fig. 13: Mean FSIM and standard error at the 30% noise level.

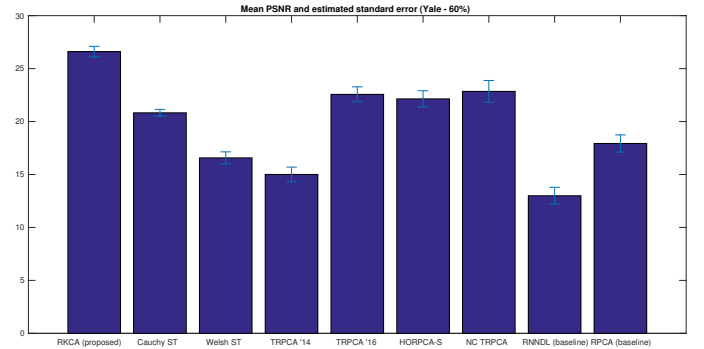


Fig. 14: Mean PSNR and standard error at the 60% noise level.

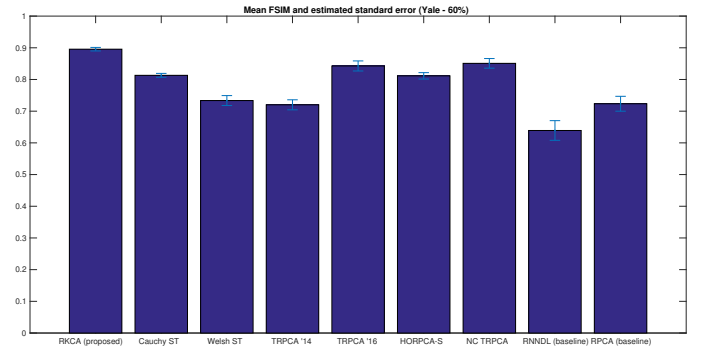


Fig. 15: Mean FSIM and standard error at the 60% noise level.

E.2 Additional denoising results on Yale

We now present supplementary denoising results. In addition to the first illumination, we show the reconstruction obtained on the third illumination, and include the output of all algorithms.

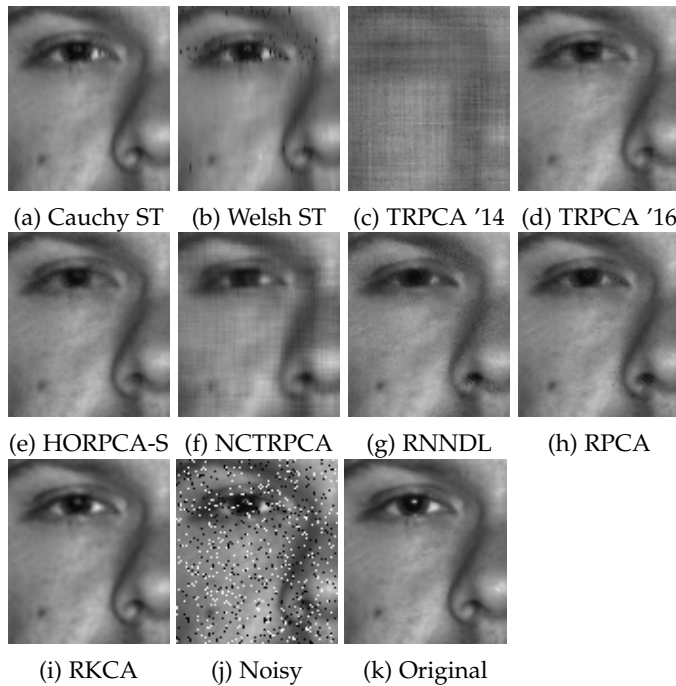


Fig. 16: Comparative performance on the Yale benchmark with 10% salt & pepper noise - first illumination.

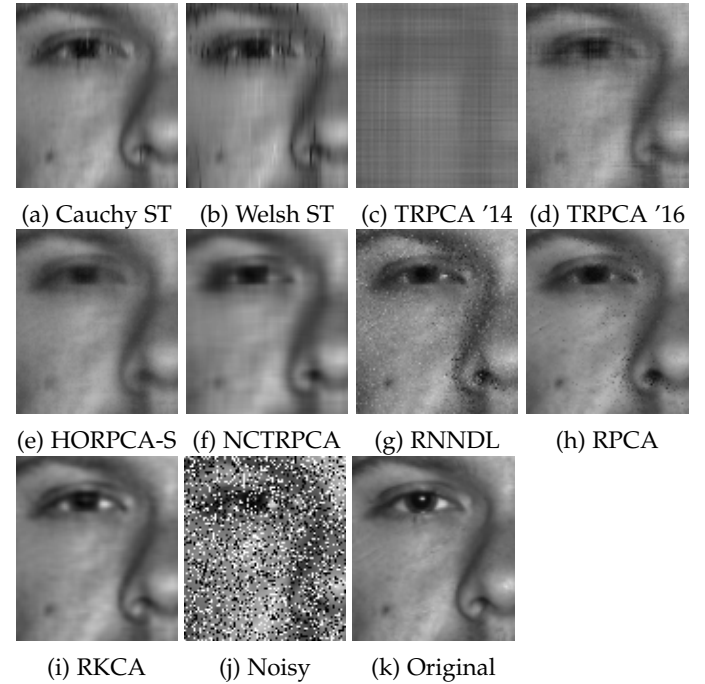


Fig. 18: Comparative performance on the Yale benchmark with 30% salt & pepper noise - first illumination.

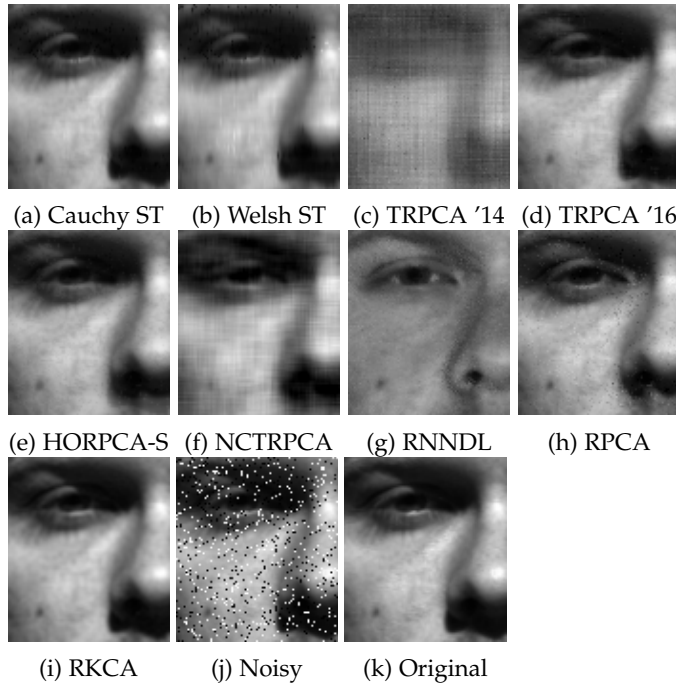


Fig. 17: Comparative performance on the Yale benchmark with 10% salt & pepper noise - third illumination.

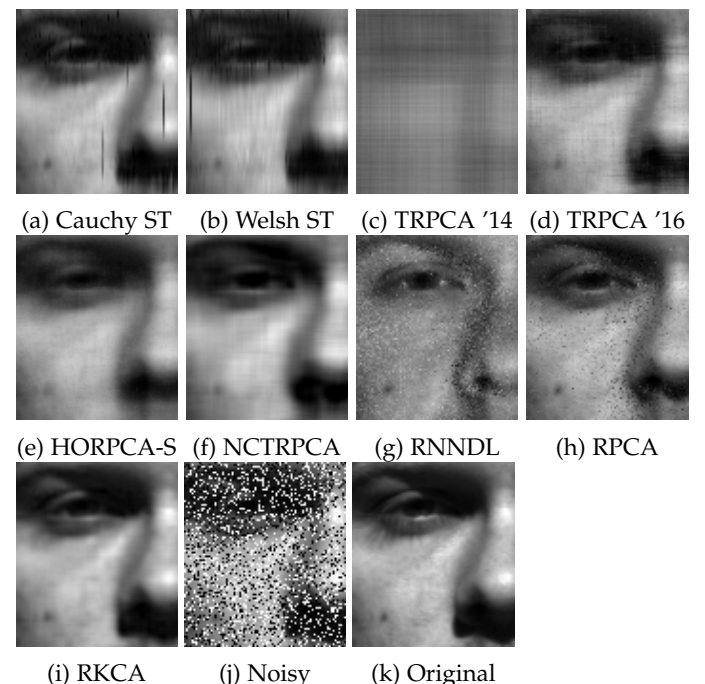


Fig. 19: Comparative performance on the Yale benchmark with 30% salt & pepper noise - third illumination.

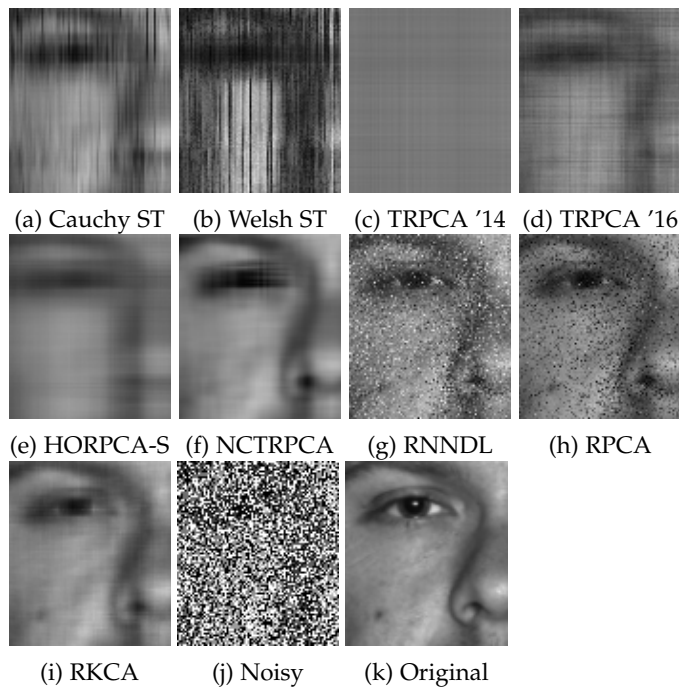


Fig. 20: Comparative performance on the Yale benchmark with 60% salt & pepper noise - first illumination.

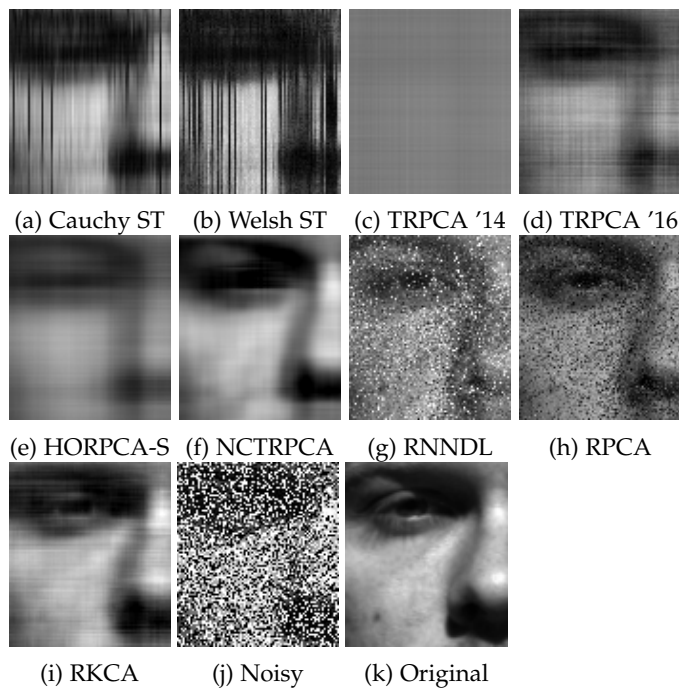


Fig. 21: Comparative performance on the Yale benchmark with 60% salt & pepper noise - third illumination.

E.3 Additional denoising results on Facade

We present the full denoising results at the 10% and 60% noise level, as well as the 30% level for completeness.

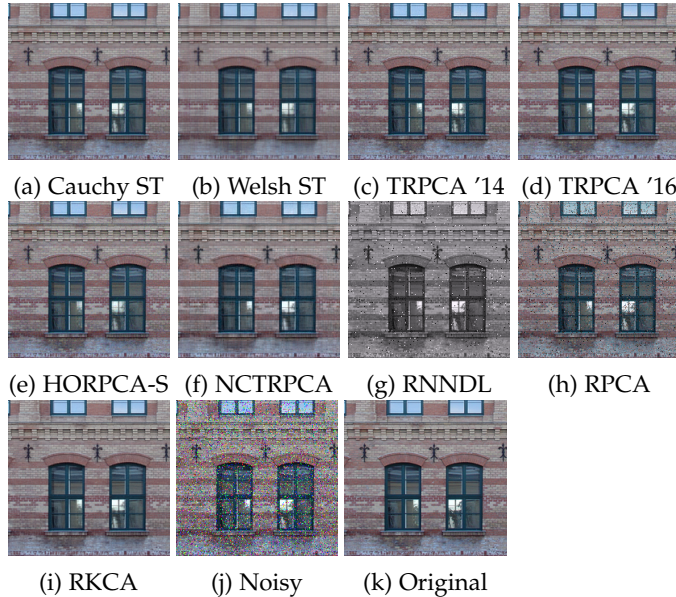


Fig. 22: Comparative performance on the Facade benchmark with 10% noise.

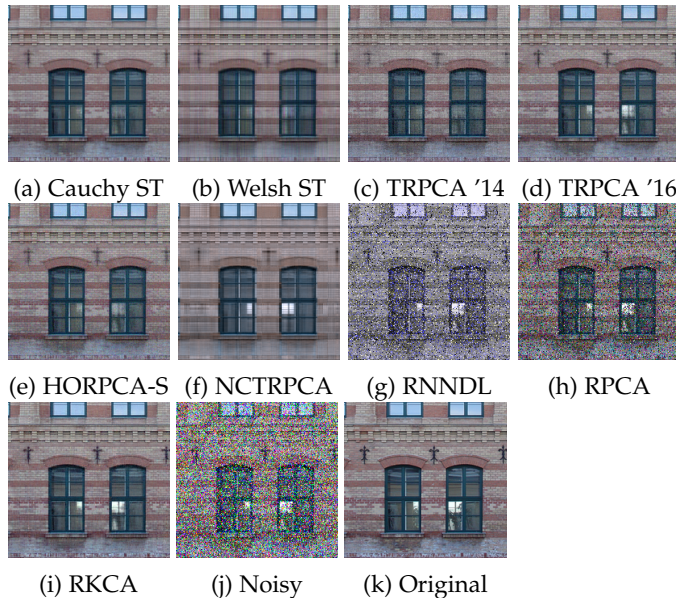


Fig. 23: Comparative performance on the Facade benchmark with 30% noise.

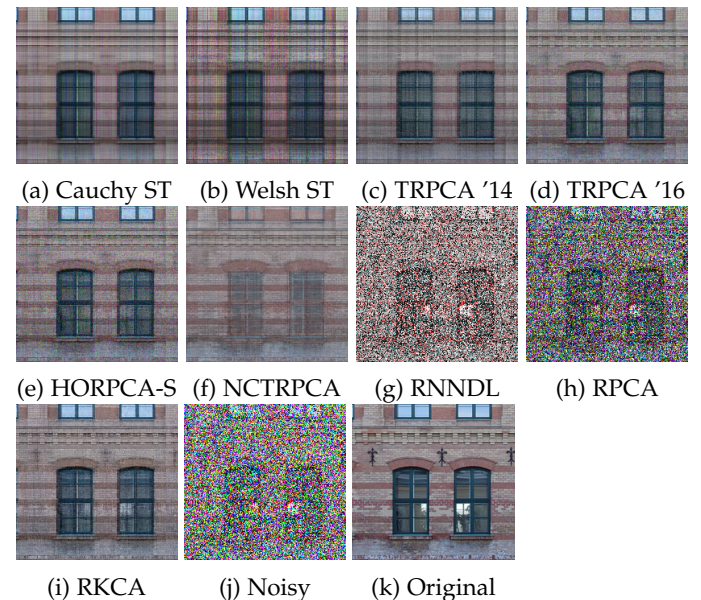


Fig. 24: Comparative performance on the Facade benchmark with 60% noise.

E.4 Background subtraction

In this Section we present the DET curves obtained on the *Highway* and *Hall* experiments, and the backgrounds obtained with each algorithm on the *Highway* benchmark.

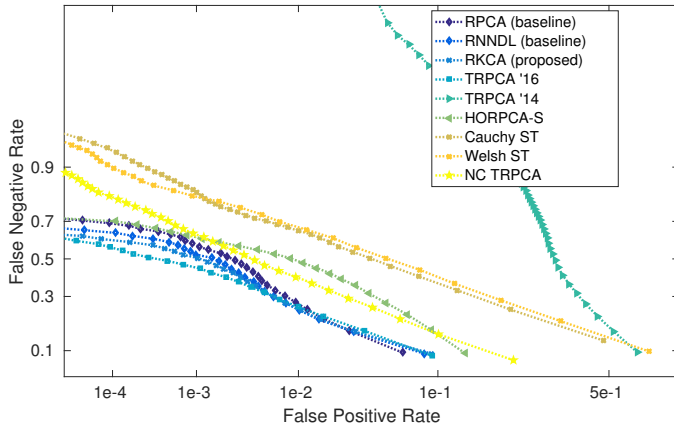


Fig. 25: DET curves on the *Highway* dataset.

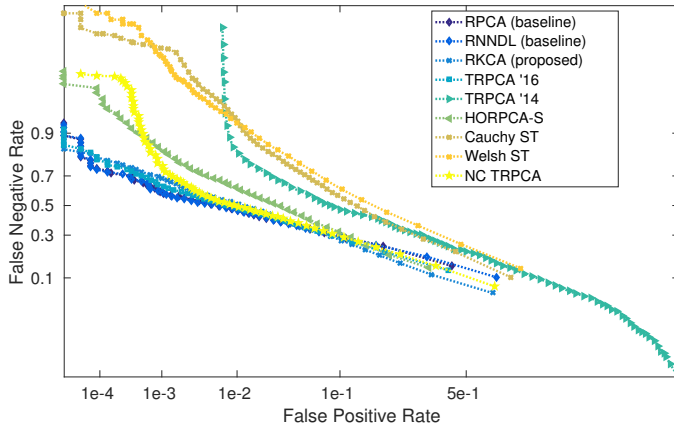


Fig. 26: DET curves on the *Airport Hall* dataset.

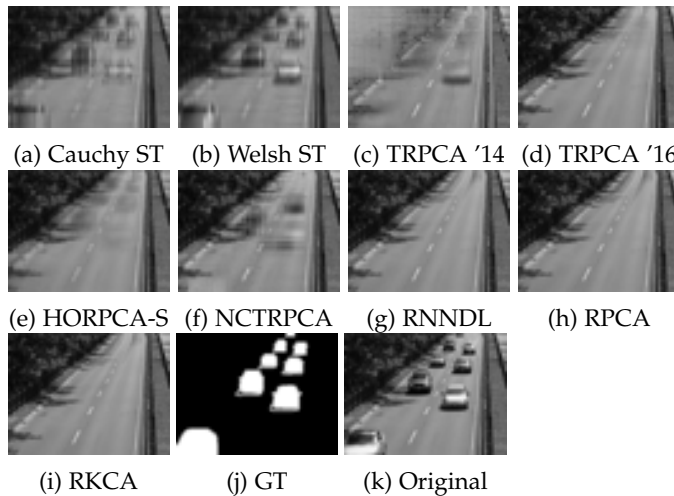


Fig. 27: Comparative performance on the *Highway* benchmark.

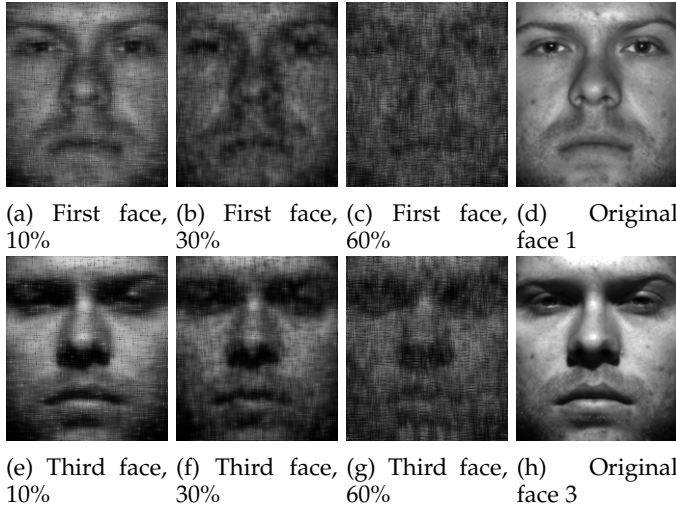


Fig. 28: Best reconstructions obtained with SeDiL on the first and third illumination according to the best overall PSNR score.

E.5 Comparison with SeDiL

We present an experiment to assess the performance of SeDiL on the Yale-B benchmark. We chose this experiment because - as presented in the original paper [15] - SeDiL is designed for denoising grayscale images.

E.5.1 Design

The data and the noise are the same as in the Yale-B experimental results presented in the paper. We describe the tuning procedure employed.

We tuned in SeDiL: κ and λ for training the dictionary, and the parameter used in FISTA for denoising that we shall denote as λ_F . In the original paper, the authors choose $\kappa = \lambda = \frac{0.1}{4w^2}$ with w the dimension of the square image patches, and $\lambda_F = \frac{\sigma_{noise}}{100}$. We tuned the parameters via grid-search, choosing:

- $\kappa = \frac{\kappa_0}{4w^2}$, $\kappa_0 \in \text{linspace}(0.05, 0.5, 5)$
- $\lambda = \frac{\lambda_0}{4w^2}$, $\lambda_0 \in \text{linspace}(0.05, 0.5, 5)$
- $\lambda_F \in 5 * \text{logspace}(-4, 0, 15)$

We kept $\rho = 100$ and patch sizes of 8×8 and extracted 40000 random patches for training from the 64 images of the first subject. We then followed the procedure described in the paper for denoising and extracted 8×8 patches in a sliding window with step size 1, denoised the patches with FISTA, and reconstructed the denoised image by averaging the denoised patches.

E.5.2 Results

We present below the results at the three noise levels: 10%, 30%, 60%. We report the mean PSNR and FSIM on the 64 images, the PSNR and FSIM on the first image, and show the reconstructions obtained.

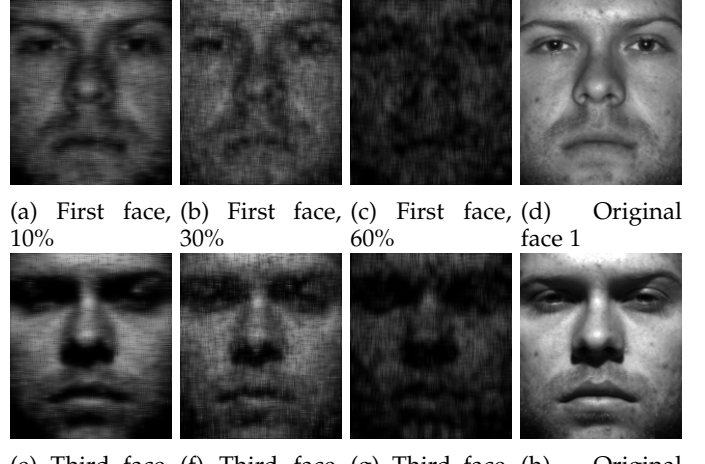


Fig. 29: Best reconstructions obtained with SeDiL on the first and third illumination according to the best overall FSIM score.

Noise level	Best PSNR face 1	Best mean PSNR	Best FSIM face 1	Best mean FSIM
10%	23.937344	23.863287	0.840798	0.862061
30%	20.988780	19.249498	0.785824	0.807403
60%	17.480783	16.095463	0.703943	0.778116

TABLE 7: Best PSNR and FSIM obtained on the first face and averaged on the 64 faces at the 3 noise levels.

E.5.3 Comments

As expected, the method is not robust to gross corruption. In all cases, the best results were obtained for $\kappa_0 = \lambda_0 = 0.5$ and $\lambda_F = 5$, indicative of the lack of robustness.